AD-A045 532 LEHIGH UNIV BETHLEHEM PA INST OF FRACTURE AND SOLID --ETC F/G 11/6
FRACTURE MECHANICS AND SURFACE CHEMISTRY STUDIES OF SUBCRITICAL--ETC(U)
SEP 77 G W SIMMONS, P S PAO, R P WEI N00014-75-C-0543

UNCLASSIFIED IFSM-77-83 NL

1 OF 2
AD A045532

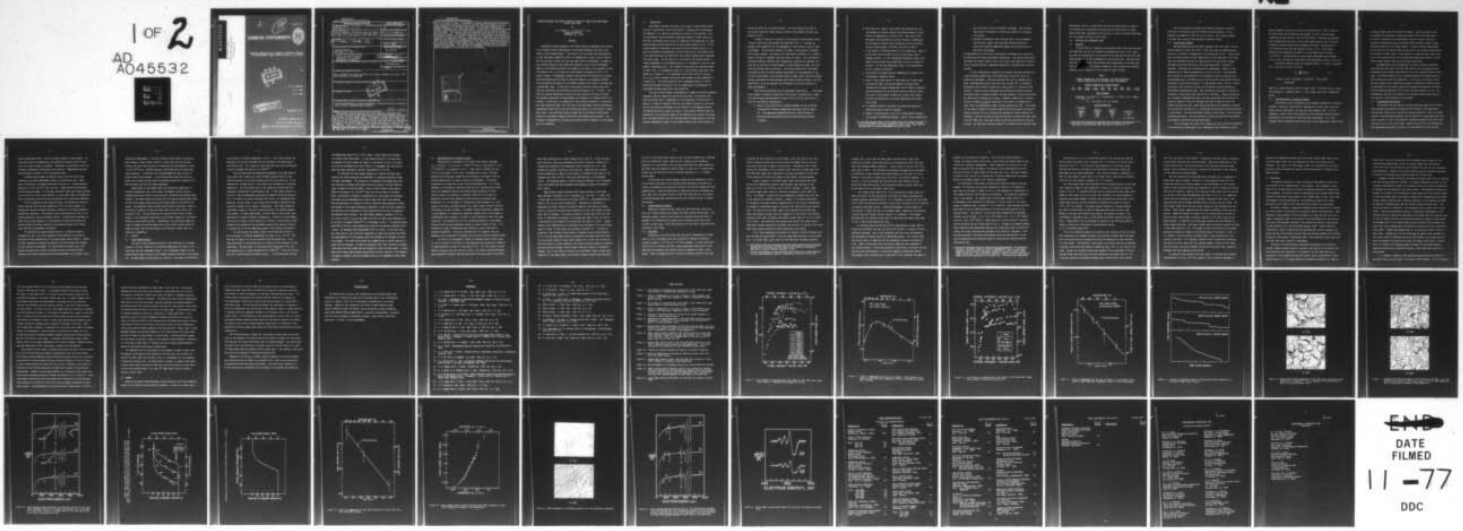

END
DATE FILMED
11-77
DDC

CONT.

INSTITUTE OF FRACTURE AND SOLID MECHANICS

IFSM-77-83

LEHIGH UNIVERSITY

FRACTURE MECHANICS AND SURFACE CHEMISTRY STUDIES OF SUBCRITICAL CRACK GROWTH IN AISI 4340 STEEL

by

G. W. Simmons

P. S. Pao

R. P. Wei

September 1977

Technical Report No. 4

Office of Naval Research

Contract N00014-75-C-0543, NR 036-097

UNCLASSIFIED

SECURITY CLASSIFICATION OF THIS PAGE (When Data Entered)

REPORT DOCUMENTATION PAGE	READ INSTRUCTIONS BEFORE COMPLETING FORM
1. REPORT NUMBER: (14) IFSM-77-83, TR-4	2. GOVT ACCESSION NO. / 3. RECIPIENT'S CATALOG NUMBER (9)
4. TITLE (and Subtitle): (6) Fracture Mechanics and Surface Chemistry Studies of Subcritical Crack Growth in AISI 4340 Steel	5. TYPE OF REPORT & PERIOD COVERED: Technical Report No. 4 / 6. PERFORMING ORG. REPORT NUMBER
7. AUTHOR(s): (10) G. W. Simmons, P. S. Pao, R. P. Wei	8. CONTRACT OR GRANT NUMBER(s): (15) Contract N00014-75-C-0543
9. PERFORMING ORGANIZATION NAME AND ADDRESS: Lehigh University, Bethlehem, PA. 18015	10. PROGRAM ELEMENT, PROJECT, TASK AREA & WORK UNIT NUMBERS: NR 036-097
11. CONTROLLING OFFICE NAME AND ADDRESS: (11) Office of Naval Research, Department of the Navy, Arlington, Virginia	12. REPORT DATE: Sep[illegible], 1977 / 13. NUMBER OF PAGES: 46 (12) 48p.
14. MONITORING AGENCY NAME & ADDRESS (if different from Controlling Office)	15. SECURITY CLASS. (of this report): Unclassified / 15a. DECLASSIFICATION/DOWNGRADING SCHEDULE

16. DISTRIBUTION STATEMENT (of this Report)

This document has been approved for public release and sale; its distribution is unlimited.

17. DISTRIBUTION STATEMENT (of the abstract entered in Block 20, if different from Report)

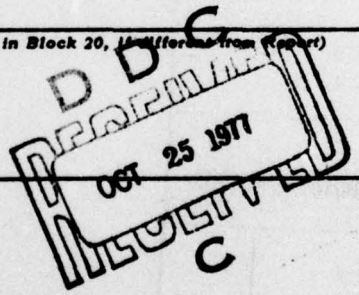

18. SUPPLEMENTARY NOTES

19. KEY WORDS (Continue on reverse side if necessary and identify by block number)

Fracture Mechanics; Surface Chemistry; Stress Corrosion Cracking; Alloy Steel; Hydrogen Embrittlement.

407 099

20. ABSTRACT (Continue on reverse side if necessary and identify by block number)

Coordinated fracture mechanics and surface chemistry experiments were carried out to develop further understanding of environment enhanced subcritical crack growth in high strength steels. The kinetics of crack growth were determined for an AISI 4340 steel (tempered at 204°C) in hydrogen and in water, and the kinetics for the reactions of water with the same steel were also determined. A regime of rate limited (Stage II) crack growth was observed in each of the environments. Stage II crack growth was found to be thermally activated, with an apparent activation energy of 14.7 ± 2.9 kJ/mol for crack growth in hydrogen, and

DD FORM 1 JAN 73 1473 EDITION OF 1 NOV 65 IS OBSOLETE

UNCLASSIFIED

SECURITY CLASSIFICATION OF THIS PAGE (When Data Entered)

33.5 ± 5.0 kJ/mol in water. Fractographic evidence indicated that the fracture path through the microstructure was the same for these environments, and suggested hydrogen to be the embrittling specie for environment enhanced crack growth in hydrogen and in water/water vapor. A slow step in the surface reaction of water vapor with steel was identified, and exhibited an activation energy of 36 ± 14 kJ/mol. This reaction step was identified to be that for the nucleation and growth of oxide. The hydrogen responsible for embrittlement was presumed to be produced during this reaction. On the basis of a comparison of the activation energies, in conjunction with other supporting data, this slow step in the water/metal surface reaction was unambiguously identified as the rate controlling process for crack growth in water/water vapor. The inhibiting effect of oxygen and the influence of water vapor pressure on environment enhanced subcritical crack growth were considered. The influence of segregation of alloying and residual impurity elements on crack growth was also considered.

FRACTURE MECHANICS AND SURFACE CHEMISTRY STUDIES OF SUBCRITICAL CRACK GROWTH IN AISI 4340 STEEL

by

G. W. Simmons, P. S. Pao and R. P. Wei
Lehigh University
Bethlehem, PA. 18015

ABSTRACT

Coordinated fracture mechanics and surface chemistry experiments were carried out to develop further understanding of environment enhanced subcritical crack growth in high strength steels. The kinetics of crack growth were determined for an AISI 4340 steel (tempered at 204°C) in hydrogen and in water, and the kinetics for the reactions of water with the same steel were also determined. A regime of rate limited (Stage II) crack growth was observed in each of the environments. Stage II crack growth was found to be thermally activated, with an apparent activation energy of 14.7 ± 2.9 kJ/mol for crack growth in hydrogen, and 33.5 ± 5.0 kJ/mol in water. Fractographic evidence indicated that the fracture path through the microstructure was the same for these environments, and suggested hydrogen to be the embrittling specie for environment enhanced crack growth in hydrogen and in water/water vapor. A slow step in the surface reaction of water vapor with steel was identified, and exhibited an activation energy of 36 ± 14 kJ/mol. This reaction step was identified to be that for the nucleation and growth of oxide. The hydrogen responsible for embrittlement was presumed to be produced during this reaction. On the basis of a comparison of the activation energies, in conjunction with other supporting data, this slow step in the water/metal surface reaction was unambiguously identified as the rate controlling process for crack growth in water/water vapor. The inhibiting effect of oxygen and the influence of water vapor pressure on environment enhanced subcritical crack growth were considered. The influence of segregation of alloying and residual impurity elements on crack growth was also considered.

1.0 INTRODUCTION

Environment assisted subcritical crack growth in high-strength steels and other high-strength alloys (particularly in hydrogen and in hydrogenous environments) is an important technological problem of long standing. Over the past decade, fracture mechanics techniques (based on linear elasticity) have been increasingly used to assist in determining the mechanisms for crack growth through characterizations of the crack growth kinetics [1-4]. In the fracture mechanics techniques, the crack-tip stress-intensity factor, K, is used to characterize the mechanical driving force and for crack growth [2-4]. It has been shown that the subcritical crack growth response may be separated into three stages. At low values of K, the rate of crack growth (da/dt) is strongly dependent on K and approaches zero as a "threshold K" value for crack growth is approached [3,4]. This regime of crack growth has been designated as Stage I [4]. At intermediate values of K, da/dt becomes essentially independent of K (Stage II). As K approaches the critical value for fracture (K_c or K_{Ic}), da/dt increases rapidly and again becomes strongly dependent on K (Stage III). The identification of the K-independent Stage II of crack growth has provided an essential link for understanding the mechanisms for environment assisted subcritical crack growth [4].

The rate of crack growth is determined by a number of possible sequential processes, with the slowest one controlling the overall crack growth rate. Since the growth rate is independent of K (the mechanical driving force) in Stage II, it must be limited by the rate of a chemical reaction, or the transport of the reacting environment, or the diffusion of the damaging species. The apparent activation energy for Stage II crack growth, therefore, must be determined by the activation energy of the underlying rate controlling process. Thus, one might identify the rate limiting process through studies of the temperature dependence of Stage II crack growth kinetics and of the kinetics of

various possible rate limiting processes. This basic approach was used in the current study and in many previous studies of environment assisted crack growth [1,5-11].

A number of studies of subcritical crack growth in high-strength steels in water, water vapor and hydrogen have been made [1,5-11]. Hydrogen was assumed to be responsible for the enhancement of crack growth in each of these environments. The activation energies for Stage II crack growth in hydrogen and in water, however, were found to be significantly different (viz., approximately 18 kJ/mol for hydrogen versus 38 kJ/mol for water). This difference in activation energies indicated that, although the interaction of hydrogen with steel may be the cause for embrittlement in both hydrogen and water, the rate limiting processes must be different. The primary objectives of the present investigation were to further develop understanding of the mechanisms of subcritical crack growth in high-strength steels in water, water vapor and hydrogen through coordinated fracture mechanics and surface chemistry studies, and, more specifically, to try to reconcile the difference in activation energies in these environments.

The following consistent set of experimental observations can be obtained from a number of studies on subcritical crack growth in hydrogen and in water for high-strength carbon-martensitic steels [1,4,5,7,12,14], and served as a basis for the present investigation:

- Stage II crack growth rate in gaseous hydrogen (at 10 to 100 kPa) increased with increasing temperature from about -80°C to about 0°C. The temperature dependence over this range followed an Arrhenius-type relationship with an activation energy of about 18 kJ/mol.

- Above about 0°C, Stage II crack growth rate departed from the low-temperature Arrhenius behavior and became essentially independent of temperature up to about +40°C. Above about +40°C, the growth rate decreased with further increase in temperature and followed an Arrhenius-type relationship with an activation energy of approximately -23 kJ/mol from +40°C to +80°C.*
- In the region of Arrhenius behavior at low temperatures, Stage II crack growth rate was found to vary with the square root of hydrogen pressure. In the intermediate temperature range, crack growth rate was found to be proportional to the first power of pressure. For the high temperature range, it was proportional to the 1.5-power of pressure.*
- Crack growth in hydrogen occurred immediately on loading, with no measurable incubation period.
- Stage II crack growth rates in liquid water and in water vapor (at pressures above 0.67 kPa and temperatures below +25°C) increased with increasing temperature, and followed an Arrhenius-type relationship with an activation energy of about 38 kJ/mol. The rates of crack growth in water and in water vapor (above 0.67 kPa and below 25°C) at any given temperature were essentially equal.
- An incubation period on the order of minutes was observed in contradistinction to that for hydrogen.
- Oxygen in concentrations of 0.6 to 0.7 volume percent arrested crack growth in humidified nitrogen. Oxygen of this concentration

---

* In the 18Ni maraging steels, a very abrupt drop off in Stage II growth rate was observed in the higher temperature region [8,9]. More detailed considerations of pressure dependence are given in [8,9].

was also found to stop crack growth in hydrogen. Once arrested, some external disturbance in loading was required to reinitiate crack growth.

- Available fractographic data indicated that in the low temperature Arrhenius region, the crack paths followed essentially along prior austenite boundaries through the microstructure for both water and hydrogen.

The mechanism(s) for subcritical crack growth in hydrogen and in water must be consistent with these experimental observations. Since these observations were made on different steels [1,5,6,7,10,11] and since there were no data on initial surface reactions, unambiguous mechanistic interpretations could not be made.

In this investigation, mechanical and chemical data were obtained on a single laboratory melted heat of AISI 4340 steel to provide a basis for mechanistic development. Data were obtained from tests in hydrogen and in water, supplementing previous data from tests in water [7], to completely characterize the kinetics of subcritical crack growth as a function of temperature. Fracture surface morphology was determined by scanning electron microscopy (SEM) to establish whether the same component of the microstructure was embrittled by hydrogen and by water. Elemental composition of fracture surfaces, produced in situ by subcritical crack growth in hydrogen and in water vapor, was determined by Auger electron spectroscopy (AES). This analysis was made to identify the surface composition and the nature and extent of chemical reaction for use in planning the appropriate surface chemistry experiments. AES was also used to study the reactions of oxygen and water vapor with AISI 4340 steel, iron (both single crystal and polycrystals), and iron carbide. The rates and activation energies of relevant surface reactions were

determined to assist in establishing the rate limiting process for Stage II crack growth and in determining the mechanism for crack arrest by oxygen. Results from these experiments and discussions in terms of possible mechanisms for crack growth are given in this paper.

2.0 MATERIAL AND EXPERIMENTAL WORK

2.1 Material

A 136 kg (300 lbs.) laboratory vacuum melted heat, with extra-low residual impurities, and an iron carbide/iron specimen were used in this study.* The steel was vacuum cast as a 10-cm-thick by 30.5-cm-wide by 56-cm-long slab ingot and was hot-rolled straightaway to 0.9-cm-thick plate. Specimen blanks were cut from hot-rolled plate and were heat treated before finish machining into test specimens. The chemical composition, heat treatment and room-temperature tensile properties of this steel are given in Table 1.

TABLE 1

CHEMICAL COMPOSITION, HEAT TREATMENT, AND ROOM TEMPERATURE TENSILE PROPERTIES OF THE AISI4340 STEEL INVESTIGATED

Chemical Composition (Weight Percent)

C	Mn	P	S	Si	Ni	Cr	Mo	Co	Ti
0.42	0.70	0.0009	0.0012	0.28	1.83	0.79	0.24	0.011	<0.005

Heat Treatment

Normalize, 1 h, 900°C, A.C. + austenitize, 1 h, 843°C, O.Q. + temper, 1 h, 204°C, A.C.

A.C. = air cool; O. Q. = oil quench

Tensile Properties

0.2% Offset Yield Strength MPa	Tensile Strength MPa	Young's Modulus GPa	Elongation Pct
1344	2082	201	9 (in 3.56 cm)

* Steel and iron carbide/iron specimens were furnished by the Research Laboratory of United States Steel Corporation, Monroeville, PA.

The iron carbide/iron specimen was prepared by heating a composite, consisting of alternating layers of Fe-6Mn alloy and graphite, in a carbonaceous environment at 1140°C for up to 14 hours. This process produced a specimen that contained large patches of cementite (Fe_3C).

2.2 Crack Growth Kinetics

Modified wedge-opening-load (WOL) specimens [13], with width = 5.23 cm and half-height to width ratio (H/W) = 0.486, were used for determining the crack growth kinetics in hydrogen and in distilled water at 0°C. (Crack growth data in distilled water at other temperatures for this same heat of AISI 4340 steel were obtained previously by Landes and Wei [7] using center cracked specimens and by Hutin and Mizuta [14] using tapered DCB -- constant K -- specimens. These data are included here for completeness. Details of the specimens used in these investigations are given in [7,14].) The specimens were oriented in the longitudinal (LT) orientation; that is, with the crack plane perpendicular to the major axis of rolling and the crack growth direction transverse to the rolling direction. A crack starter notch, 1.52 cm in length and having a root radius of 0.25 mm, was introduced into each specimen by electrospark discharge machining. Each specimen was precracked in fatigue to introduce a 0.25-cm-long crack from the tip of the notch. Fatigue precracking was initiated in dehumidified argon, and final precracking was carried out in vacuum (at about 10^{-4} kPa) at a maximum load equal to about 75 pct of the planned starting test load. Both fatigue precracking and subsequent sustained-load testing were carried out in a closed-loop electrohydraulic machine operated in load control. Load was maintained constant to better than ± 1 pct during the sustained-load tests. Load was applied to initiate the test after the desired environmental conditions had been established.

Test environment and control for hydrogen, and the dc electrical potential crack monitoring systems used in this investigation were identical to those

used by Gangloff and Wei [9], and are not described here. Tests in water at 0°C were carried out by immersing the specimen in triply distilled water containing ice made from the triply distilled water. The water was deaerated with nitrogen during the test, and the space above the water was filled with nitrogen to minimize absorption of oxygen by the water. Temperature stability during a given test was typically within ± 1.5°C. Crack length resolution was estimated to be about 10 μm, and growth rate resolution, 2×10^{-8} m/s. The uncertainty for crack length measurements was estimated to be ± 3 pct, and that for crack growth rate measurements, about ± 20 pct [9].

The stress intensity factor was computed from Eq. (1), which is accurate to ± 1 pct for $0.3 \leq a/W \leq 0.75$ [13].

$$K_I = \frac{P\sqrt{a}}{BW} Y(a/W) \qquad (1)$$

$$Y(a/W) = 30.96 - 195.8(a/W) + 730.6(a/W)^2 - 1186.3(a/W)^3 + 754.6(a/W)^4$$

where K_I = stress intensity factor for mode I [16]; P = applied load; B = specimen thickness; W = specimen width; a = crack length; and Y(a/W) = geometrical factor.

2.3 Characterization of Fracture Surfaces

The technique used for determining the elemental composition of fracture surfaces, produced by crack growth in hydrogen and in water vapor inside the Auger electron spectrometer, has been described elsewhere [15]. For this technique, a special device was designed to allow sustained-load crack growth experiments to be carried out inside the Auger spectrometer. All of the *in situ* fracture experiments were carried out at room temperature by back-filling

the Auger chamber with the selected environment. High purity water vapor was obtained by alternately freezing and thawing triply distilled water in a side-arm, connected to the spectrometer through a variable leak valve. Hydrogen was obtained by passing ultrahigh purity hydrogen through a heated palladium thimble into the vacuum chamber. To ensure accurate measurements of the extent of the reaction that had occurred at the fracture surface during crack growth in water vapor, it was essential to reduce the water vapor pressure in the system into the low μPa range before making AES analysis to avoid electron beam induced reactions with residual water vapor.

Characterization of the morphology of fracture surfaces, produced by sustained-load crack growth (for both the kinetics and the in situ fracture experiments) and by impact, were made with the aid of scanning electron microscopy. The entire broken halves of selected specimens were placed inside an ETEC Autoscan microscope for examination. In this way, the location on the fracture surface can be identified and specific morphological features could be correlated with the kinetic data and the appropriate mechanical variables. The microscope was operated at 20 kV with a working distance of 11 mm. The specimen was tilted 25° with respect to the incident electron beam, about an axis parallel to the direction of crack growth.

2.4 Surface Reaction Kinetics

The kinetics for the reactions of water vapor and oxygen with AISI 4340 steel surfaces were obtained by measuring the increase in the oxygen Auger electron peak intensity as a function of exposure (pressure x time) in a manner similar to that described previously for the reactions of these gases with iron single crystals [17,18]. A polished and ion-etched specimen of AISI 4340 steel (0.08 cm x 0.5 cm x 2.0 cm) was used. (Based on results from the characterization experiments described in section 3.2, the composition of this surface

closely approximates that of fracture surfaces exposed by crack growth). For experiments above room temperature, the specimen was heated directly by passing a dc current through the specimen. Temperature was monitored by an iron-constantan thermocouple spot-welded to the specimen. Temperatures were maintained constant to within ± 2°C of the desired values.

Ultrahigh purity oxygen was obtained from an one-liter Pyrex flask connected to the Auger spectrometer through a variable-leak valve. Water vapor was obtained in the manner described in section 2.3. Flowing oxygen at pressures up to 133 μPa (10^{-6} torr) was used. Oxygen pressure was monitored with an ionization gauge. For reactions with water vapor, much higher pressures (up to 0.67 kPa or 5 torr) were required. A static water vapor environment was used, and the water vapor pressures were measured with a capacitance manometer.

Prior to exposures to the respective gases, the specimen was argon ion etched (1000 eV) until the base composition of the alloy was reached. No evidence was found for surface enrichment or depletion of alloying elements by preferential sputtering. The reaction kinetics were measured for the as ion-etched (atomically rough and strained) surface. Following each experiment in water vapor at high pressures, it was necessary to outgas the specimen and specimen holder to minimize reaction of the specimen surface with residual water vapor during subsequent ion etching.

For measuring the oxygen reaction kinetics, a cumulative exposure procedure was used. The flow of oxygen was interrupted and the system was evacuated for each determination of the oxygen Auger signal intensity. Oxygen was then readmitted to continue the exposure, and the procedure was repeated for each successive measurement. For the reaction with water vapor, each exposure was made from a freshly ion-etched surface to eliminate effects induced by the incident beam during previous measurements and, thereby, ensure

reproducible measurements. Since the incident electron beam of the spectrometer tended to induce further reaction of water vapor with the specimen surface, the effect was minimized by re-evacuating the spectrometer to below 1.33 μPa (10^{-8} torr), following exposure, before measuring the oxygen Auger signal intensity. In addition, only one measurement was taken at each of several areas of the specimen. To avoid beam induced reactions during exposure, the incident electron beam for the Auger analyzer was turned off for both the water vapor and the oxygen experiments.

Normalization of the oxygen signal was required for comparisons of different experimental runs, since various instrumental factors (such as specimen position and electron multiplier gain) influenced the absolute signal strength. The oxygen signal was normalized by dividing the peak-to-peak height for the 510 eV oxygen signal by the peak-to-peak height for the 605 eV iron signal. The normalized signal has been quantitatively calibrated in terms of the extent of reaction of oxygen and water vapor with single crystal iron surfaces [17,18]. The quantification for annealed single crystal surface, however, is not necessarily applicable to the present studies with ion etched surfaces of polycrystalline steel. Nevertheless, the normalized oxygen/iron signal is expected to provide comparisons of the relative reaction rates of oxygen and water vapor and the changes in the reaction of water vapor as a function of temperature.

3.0 RESULTS

3.1 Crack Growth Kinetics

The results from sustained-load test of AISI 4340 steel at a hydrogen pressure of 133 kPa (1000 torr) for different temperatures are shown in Fig. 1. These data show the K dependent (Stage I) and K independent (Stage II) crack growth behavior that is typical of environment enhanced subcritical crack growth [4]. The mean Stage II crack growth rate from Fig. 1 are shown as a function of

the reciprocal of absolute temperature in Fig. 2. Error flags indicate the magnitude of the 90 pct confidence interval estimate of the mean Stage II crack growth rate. The K-range over which each mean rate value was measured typically extended from about 40 to 70 MPa-$m^{1/2}$.

The curve describing the temperature dependence of the mean Stage II crack growth rate is made up of three different regions similar to that reported previously by Williams and Nelson for AISI 4130 steel [5]. At low temperatures, the mean Stage II crack growth rate increased with increasing temperature. The crack growth rate in this region can be described by an exponential relationship of the Arrhenius type. A least square analysis of the data in the low temperature region gave an apparent activation energy of 14.7 ± 2.9 kJ/mol on a 90 pct confidence level basis. At intermediate temperatures, the mean Stage II crack growth rates attained a maximum and were essentially insensitive to changes in temperature. This region apparently represented a change in the rate controlling process for hydrogen enhanced crack growth. At higher temperatures, the mean Stage II crack growth rates decreased with further increases in temperature. Although all three temperature regions of Stage II crack growth are of interest in developing an understanding of the mechanisms for environment enhanced crack growth, attention is focused only on the low temperature region in the present investigation.

The crack growth rate versus K data for AISI 4340 steel tested in distilled water at different temperatures are shown in Fig. 3 [7,14]. Only the data for Stage II at 0°C were obtained from the present work. Fig. 4 shows mean Stage II crack growth rate as a function of the reciprocal of test temperature. The mean Stage II crack growth rate values used in this plot were measured over a K-range from about 30 to 70 MPa-$m^{1/2}$. Error bars on each data point indicate 90 pct confidence interval. In distilled water and over

the temperature range of 0°C to 75°C, Stage II crack growth rate followed an Arrhenius-type relationship. A least squares analysis of the data gave an apparent activation energy for Stage II crack growth of 33.5 ± 5.0 kJ/mol (on a 90 pct confidence level basis) which is in agreement with the value of about 38 kJ/mol reported by previous investigators [1,7,10,19].

An indication of crack growth response as a function of water vapor pressure and stress intensity was determined in a separate experiment inside the Auger spectrometer. The purpose was to determine the minimum vapor pressure required to produce crack growth within the range of K-values found for Stage II growth in distilled water. With an initial vacuum in the spectrometer on the order of 0.1 μPa (10^{-10} torr) and with a source of ultrapure water, the possible influence of contamination on crack growth was minimized. The output of the instrumented bolt used to apply the load to the specimen [15] was monitored as a function of time at different vapor pressures of water. The changes in this output (produced by decreases in load with crack extension) was used only as an indication of crack growth and was not used for measuring the absolute rate of growth. The crack growth response, observed at 13.3 Pa (0.1 torr), 133 Pa (1.0 torr) and 1064 Pa (8 torr) of water vapor pressures for an initial K_I of about 50 MPa-$m^{1/2}$, is illustrated in Fig. 5. At pressures above about 670 Pa (5 torr), crack growth was relatively fast and was essentially continuous. At pressures below approximately 670 Pa (5 torr), on the other hand, the crack grew at a very slow rate (comparable to creep crack growth rates [20]) for approximately 15 to 20 minutes, which was followed by an increment of rapid crack growth. This rapid crack growth was accompanied by an audible emission of sound from the specimen. At these low pressures, the K level required to produce crack growth was much higher than the threshold K value for crack growth in liquid water and in water vapor pressures above 670 Pa (5 torr) (see Fig. 3 for example). It appears, therefore, that the threshold value of K is dependent on water vapor pressure.

3.2 Characterization of Fracture Surface

Representative fractographs of AISI 4340 steel tested in hydrogen (P_{H_2} = 133 kPa, T = 22.2°C and K = 33 MPa-$m^{1/2}$) and in liquid water (T = 0°C, K = 33 MPa-$m^{1/2}$) are compared in Fig. 6. These results indicate that subcritical crack growth in this steel, in hydrogen and in water, followed essentially the same path through the microstructure, and suggest that the cracking mechanism was the same in these two environments. The surface morphology can be described by the following characteristics: (1) a large component of intergranular separation along the prior austenite grain boundaries; (2) deformation markings and apparent phase decohesion on intergranular facets; (3) subcracks or secondary cracks out of the plane of macroscopic fracture that apparently follow along prior-austenite grain boundaries; (4) a finite amount of transgranular quasi-cleavage (i.e., with respect to the prior austenite grains); (5) a small amount of ductile tearing, often mixed with quasi-cleavage. The bimodal fracture morphology, composed of a large component of intergranular separation combined with a finite amount of transgranular quasi-cleavage, is similar to that reported for other iron based alloys [6]. The susceptibility of prior austenite boundaries to environment induced failure has been documented already in several studies [21-24]. It is reasonable to expect transgranular quasi-cleavage to occur along massive martensite boundaries. Since such interfaces were not observed, they are apparently less susceptible to hydrogen than the prior austenite boundaries [22].

The results of fractographic studies of specimens tested in water vapor at 0.67 to 1.06 kPa (5 to 8 torr) at room temperature were essentially identical to those described for tests in liquid water at 0°C. For crack growth in water vapor at pressures less than 0.67 kPa (5 torr), the fracture surface morphology was considerably different from that associated with crack growth at the higher

water vapor pressures and in water (compare Figs. 6 and 7a). At the low water vapor pressures, there was considerably more ductile tearing in comparison to intergranular separation and transgranular quasi-cleavage (Fig. 7a). Some evidence of secondary cracking was also observed. Comparison with fracture surface morphology for Stage III crack growth or overload failure (see Fig. 7b) suggested that these "brittle" facets were manifestations of environmental effects. The extensive amounts of ductile tearing reflected, in all likelihood, creep crack growth [20] that accompanied environment assisted crack growth at high K levels.

Auger electron spectra obtained from fracture surfaces of AISI 4340 steel specimens fractured in situ in hydrogen (P_{H_2} = 53.2 kPa, T = -30°C), and in water vapor at 0.67 kPa and at less than 0.67 kPa (T = room temperature) are shown in Figs. 8a, 8b, and 8c respectively. There were no indications of segregation of either alloying or residual elements on the fracture surfaces (that is, along prior austenite grain boundaries) of the steel tested in either water vapor of hydrogen. The extent of reaction of water vapor with AISI 4340 steel, as indicated by the height of the oxygen peak shown in Figs. 8b and 8c, is equivalent to the formation of not more than two layers of "oxide". Further details on the formation and on an estimate of the thickness of this passivating layer of "oxide" in water vapor are described in section 3.3. The extent of oxidation of the fracture surface tested in hydrogen (caused by backstreaming of air into the spectrometer during re-evacuation) was greater than that found for the surfaces exposed to water vapor (compare Fig. 8a with Figs. 8b and 8c). While the amount of "oxide" formed on the fracture surfaces produced in hydrogen may have obscured the Auger electron signal from small amounts of segregated elements, this is not likely to be the case for specimens tested in water vapor. Comparison of the Auger spectra from fracture surfaces produced above and below

0.67 kPa (5 torr) water vapor pressure, Figs. 8b and 8c respectively, indicated that iron carbide was present along the prior austenite grain boundaries. Phosphorus, tin and antimony, that have been associated with temper embrittlement [25], were not observed on these surfaces; at least not in concentrations greater than the sensitivity limit of the AES technique (~0.1 - 1.0 atomic percent [26]).

The fact that the surface analyses showed that the composition of fracture surfaces (principally prior austenite grain boundaries) contained iron carbide, but otherwise was essentially identical with the bulk composition [15], suggested that it would be appropriate to study the reactions of hydrogen and water vapor with ion-etched surfaces of AISI 4340 steel and with iron carbide to evaluate whether these reactions were the rate controlling step in Stage II crack growth.

3.3 Surface Reaction Kinetics

Reactions of oxygen and water vapor with AISI 4340 steel surface and with iron carbide surfaces were studied with Auger electron spectroscopy. This technique, however, cannot be used either for studying surface reactions of hydrogen or for determining the disposition of hydrogen during the surface reaction of water vapor. Only those reactions for which AES is applicable were considered in this study.

3.3.1 AISI 4340

According to an earlier study [18], the initial chemisorption of water vapor on iron is extremely rapid and is essentially complete following an exposure of about 7×10^{-4} Pa-s (5×10^{-6} torr-seconds). At water vapor pressures of 0.67 to 1.06 kPa (5-8 torr), where appreciable crack growth in AISI 4340 steel was observed, this reaction would be completed in about 1 microsecond. Taken in conjunction with an observed incubation period of the order

of minutes for the initiation of crack growth in this steel [4,14], this fast initial reaction of water vapor with the steel was deemed unlikely to be the rate controlling step for Stage II crack growth. Although this fast initial reaction was considered to be an essential step, reactions of water vapor with AISI 4340 steel beyond this chemisorption step were considered to be the more likely reactions for controlling Stage II crack growth, and were examined.

Further increases in the (O/Fe) Auger signal ratio beyond that found for the fast chemisorption reaction required water vapor exposures on the order of 1.33 to 1.33 x 10^3 kPa-s (10 to 10^4 torr seconds). Figure 9 shows the (O/Fe) Auger signal ratio as a function of exposure* at 25°C, 100°C and 175°C. The changes in reaction rate with temperature indicated that this step of the reaction was thermally activated. Changes in the energy distribution of low energy iron Auger electrons suggested that an iron oxide or oxyhydroxide (as opposed to chemisorbed oxygen or hydroxyls) was formed during this reaction step. The value for (O/Fe) Auger signal ratio observed for AISI 4340 steel after high exposure to water vapor was comparable to that found on the fracture surfaces of this steel following crack growth in water vapor at 0.67 to 1.06 kPa (5 to 8 torr). The relatively high exposure required for this second step of water-metal surface reaction was consistent with the 0.67 to 1.06 kPa (5 to 8 torr) water vapor pressure required to obtain appreciable crack growth.

At all three temperatures the oxide film reached a limiting thickness that was less than the escape depth of iron and oxygen Auger electrons in iron oxide** [17]. The (O/Fe) Auger signal ratio for AISI 4340 steel following saturation

---

* The reaction rates for both water vapor and oxygen were found to be directly proportional to pressure, and the kinetics are, therefore, conveniently described in terms of exposure (pressure x time).

** The mean escape depth of iron and oxygen Auger electrons for oxide formed on iron by room temperature exposure to oxygen was found to be 70 nm [17].

exposure, Fig. 9, was about two times higher than the (O/Fe) signal ratio observed on a Fe(001) surface passivated by an one-atom-layer thick "FeO-like" layer that had been formed by heating a single crystal in 133 μPa (10^{-6} torr) water vapor at 500°C. The difference in the amount of oxygen may be attributed to differences in the nucleation and growth process for the oxide, or to differences in the extent of hydration of the oxide, or to surface roughness. In any case, it can be concluded that the oxide layer that formed on the ion-etched AISI 4340 steel surface, after saturation exposure to water vapor, was on the order of one to two atomic layers thick.

The S-shape curves shown in Fig. 9 for the reaction of water vapor with steel are similar to those observed for the kinetics of phase transformations through nucleation and growth [27-30]. It is reasonable to expect that the formation of oxide film during the reaction of water vapor with steel also took place by a nucleation and growth process. Detailed development of kinetic models for this process is beyond the scope of the present paper. Modeling of the reaction of water vapor with Fe(001) surface, however, is in progress. The concepts developed thus far provide a useful basis for describing the kinetic data shown in Fig. 9, and are described briefly here.

It has been shown [18] that the initial chemisorption of water vapor on Fe(001) was disordered, and that only 80% of the available sites were filled at saturation coverages. Most of the unoccupied sites were along the boundaries that separated the domains covered by chemisorbed species. This initial chemisorption was rapid in comparison with the subsequent nucleation and growth of oxide. Based on these data [18], the following model has been suggested for the oxidation process. During high exposures to water vapor, the oxides nucleate and grow along the boundaries of preexisting domains of chemisorbed species. These domains have a distribution of sizes which in turn determine the number of

boundary sites available for oxidation. Since the final oxide thickness is limited, the lateral growth of the oxide is much faster than growth normal to the surface and, therefore, predominates. Kinetic equations can be derived for this model by assuming that the shapes of the domains can be approximated by circles and that the rate of lateral growth of the oxide layer (viz., the rate of change of radius of the circles) is a constant and is directly proportional to pressure. Details of the model, however, still need to be developed.

For the purpose of this paper, a Gaussian distribution of domain sizes was assumed. The fraction of the surface converted to oxide (θ) as a function of β(pt) given by the model is shown in Fig. 10. The parameter β is proportional to the standard deviation for the Gaussian distribution. The product pt (pressure x time) is the exposure. By assuming that an (O/Fe) Auger signal ratio of 0.7 corresponded to the initiation of oxidation (θ = 0) and a ratio of 1.40 corresponded to completed layer of oxide (θ = 1.0), values for β were obtained from the data shown in Fig. 9 by minimizing errors in θ over the rising portion of the reaction curves. The values of β, along with the estimated 90 pct confidence interval, are as follows: $(2.3 \pm 1.0) \times 10^{-6}$ (25°C); $(3.5 \pm 1.7) \times 10^{-5}$ (100°C); and $(3.3 \pm 2.0) \times 10^{-4}$ (175°C).* These values are in units of $(Pa\text{-}s)^{-1}$ and were used to construct the solid lines shown in Fig. 9. Although the agreement between model predictions and experimental data was not exceptionally good, the model did reflect the correct trend and was considered to be physically reasonable. Since the model provided a consistent and systematic basis for data analysis, it was used for determining the activation energy for the oxidation reaction from the experimental data.

* The 90 pct confidence intervals represent pro forma estimates. An alternative procedure, involving minimizing errors in exposure (pt) over the same range, tended to favor the data at the higher exposures and yielded proportionately higher values for β. This alternative procedure, however, did not significantly change the relative positions of the curves (viz., the temperature dependence).

By plotting ln β vs 1/T, an activation energy for the reaction was obtained and was found to be equal to 36 ± 14 kJ/mol (8.7 ± 3.4 kJ/mol) on a 90 pct confidence basis (Fig. 11). The relatively large uncertainty in activation energy resulted from the fact that material and experimental constraints limited the measurement to only three temperatures. This activation energy is comparable to that for crack growth in water (33.5 ± 5.0 kJ/mol) and is significantly different from that for crack growth in hydrogen (14.7 ± 2.9 kJ/mol).

The (O/Fe) Auger signal ratio obtained from an ion-etched surface of AISI 4340 steel exposed to oxygen at room temperature is shown as a function of oxygen exposure in Fig. 12. In contradistinction with the reactions with water vapor, which formed an oxide layer of one to two atom layer thickness, the oxide produced by reactions with oxygen reached a thickness that approached the escape depth of the oxygen Auger electron (∿70 nm) following an exposure of the order of 10 mPa-s (0.75×10^{-4} torr second). The oxygen exposure required to initiate oxidation was found to be more than six orders of magnitude below that for water vapor. Because of the very rapid reaction with oxygen, the presence of oxygen in the environment is expected to form a surface oxide and inhibit reaction with water vapor. These results will be considered in relation to the inhibiting effect of oxygen on subcritical crack growth in the discussion section.

3.3.2 Iron Carbide (Fe_3C)/Iron

Since iron carbide was shown to be present on the fracture surfaces (or along prior austenite grain boundary surfaces), the reactions of water vapor and oxygen with iron carbide were also examined to assess the importance of these reactions for crack growth. Unfortunately, single phase iron carbide could not be obtained. A specimen containing large patches of cementite (Fe_3C), Fig. 13, was used for this study. Because the incident electron beam diameter of the spectrometer (∿500 μm) was much larger than the size of the iron carbide and iron phases (see Fig. 13), it was not possible to distinguish between carbon that may be in solid solution

with iron from carbon in iron carbide. Consequently, detailed kinetic information on the surface reactions could not be obtained. Qualitative comparisons of the relative reactivity of iron carbide and pure iron with water vapor and oxygen, however, could be obtained and used in assessing the importance of the reactions of iron carbide with the environment.

The iron carbide and iron specimens were ion-etched prior to exposures to either water vapor or oxygen. Although it is not known what effect this ion etching may have had on inducing changes in the stoichiometry of iron carbide, studies of the ion-etched surface may, nevertheless, give an indication of the details of this reaction. Results of the reaction of water vapor with iron carbide at 0.67 kPa (5 torr) and room temperature are shown in Fig. 14. For comparison, results from an ion-etched pure iron specimen, (exposed to water vapor at the same time) and from the carbide specimen during ion etching are also shown. The (O/Fe) Auger signal ratio from the reacted surfaces of both specimens were comparable. These results suggested that the extent of oxidation in each case was similar. Comparison between the spectra for iron carbide before and after exposure to water vapor showed an apparent reduction of the carbon signal by the water reaction. In addition, the carbon Auger electron peak was examined at a higher energy resolution. The results showed that the reaction produced splitting of the carbon peak (Fig. 15). This change in energy distribution of the carbon peak may be caused by a change in the binding energy of the carbon 1s level, or by a change in the distribution of energy states in the valence band of iron carbide, or by both. It is apparent, therefore, that in addition to oxidation, the reaction of water vapor with iron carbide removed a fraction of the carbon from the surface, and also converted a fraction of the carbon into a chemically different form that remained on the surface.

In contrast to the reaction with water vapor, a relatively short exposure (approximately 0.27 Pa-s x 10^{-3} torr second) of the iron carbide specimen to

oxygen at room temperature reduced the carbon Auger electron peak almost to zero. The (O/Fe) Auger signal ratio was comparable for both iron carbide and iron specimens. The value of the (O/Fe) Auger signal ratio indicated that the oxide thickness on both specimens was greater than the escape depth of oxygen and iron Auger electrons.

4.0 DISCUSSION

The combined influences of stress and chemical environment on subcritical crack growth in high strength steels is very complex. Many fundamental issues remain to be resolved before an universally acceptable mechanism (or mechanisms) can be proposed. The results from this investigation have provided further understanding of subcritical crack growth in high strength steel in water, water vapor and hydrogen, and have contributed to the resolution of some of the issues, particularly with respect to the rate controlling process for crack growth.

Any one of a number of sequential processes may be responsible for limiting the rate of Stage II crack growth in an external chemical environment [9]. These processes include transport of the environment to a region near the crack tip, a number of sequential steps in the reaction of the environment with the crack surface, entry and subsequent transport of the embrittling species to the fracture (or embrittlement) site, and the fracture process itself. Results from this investigation, taken in conjunction with published data in the literature, suggested that one of the surface reaction steps was the most probable rate limiting process for crack growth in water/water vapor. The reactions of water vapor with AISI 4340 steel were, therefore, investigated.

Analyses of fracture surfaces indicated that segregation of alloying or residual elements (except possibly of carbon in the form of iron carbide) to the prior austenite grain boundaries is not essential for AISI 4340 steel to be susceptible to environment assisted crack growth, unless concentrations of such elements below 0.1 to 1.0 atomic percent can determine susceptibility. Based on

these results, one can conclude that the environments react essentially with surfaces having compositions similar to the bulk composition (principally iron in this case) and possibly with iron carbide at or near the prior austenite grain boundaries. Studies of the surface reaction kinetic, therefore, were made principally on polished and ion-etched surface of AISI 4340 steel.

A number of studies [31-35] of the reaction of water vapor with iron indicate that the following steps are involved: (1) physical adsorption of water, (2) dissociative chemisorption of water, (3) oxidation of the iron surface and liberation of hydrogen and (4) hydration of the oxide surface. This sequence of reactions is expected to be similar for the reactions of water vapor with iron carbide, except in this case methane and/or the oxides of carbon may be produced during the chemisorption and/or oxidation steps. Physical adsorption is not thermally activated, and physically adsorbed water does not interact strongly with the steel. This step of the reaction, therefore, is not expected to play a direct role in crack growth. Since the chemisorption reaction is essentially instantaneous at the pressures that are required for appreciable crack growth [18], this reaction step is also not likely to be the rate controlling process for Stage II crack growth. The decomposition of iron carbide along the prior austenite grain boundaries by water vapor and by hydrogen may be considered as plausible cause for subcritical crack growth. Indeed, some decomposition of iron carbide was shown to occur in water vapor. Decomposition of iron carbide per se, however, does not appear to be a direct cause for enhancing subcritical crack growth, since oxygen was also shown to decompose the carbide and yet does not enhance crack growth. Furthermore, the formation of oxide per se does not appear to cause embrittlement, otherwise oxygen would be expected to enhance, rather than arrest subcritical crack growth.

It is apparent, therefore, that hydrogen produced during the reaction of the steel surface in water vapor is the cause of embrittlement. This is consistent

with the observed similarity in the fracture surface morphology for specimens cracked in hydrogen and in water. The agreement between the activation energy for Stage II crack growth (33.5 ± 5.0 kJ/mol) and the activation energy for the nucleation and growth of the oxide in water vapor (36 ± 14 kJ/mol) suggests that the hydrogen responsible for embrittlement is produced during this oxidation reaction, and indicates that the oxidation reaction is the rate limiting process for crack growth. The results of this study suggest that the difference in apparent activation energies for Stage II crack growth in hydrogen and in water for AISI 4340 steel is caused by the fact that the activation energy for the oxidation reaction and production of hydrogen in water is higher than the activation energies for the surface reactions of hydrogen and/or transport of hydrogen in the steel. Which one of these later processes is responsible for controlling crack growth in hydrogen remains to be determined. Similar studies of the reactions of water with iron carbide are required to determine whether hydrogen produced during these reactions may also contribute to crack growth. A specimen containing much larger carbide phases (~500 μm) or an Auger spectrometer with a smaller diameter incident electron beam than those used in this investigation, however, would be required.

Crack growth in water vapor at pressures below about 0.67 kPa (5 torr) occurred as a series of rapid growth increments interspersed by slow creep crack growth. The fracture surface moephology indicated that crack growth occurred by a relatively high proportion of ductile-dimple failure, with minor amounts of "brittle" facets. At water vapor pressures have about 0.67 kPa (5 torr), continuous crack growth was observed, and the fracture morphology indicated that the major failure mode was intergranular. Changes in crack growth behavior as a function of water vapor pressure has been reported previously by Johnson and Willner on a H-11 steel [1]. These investigators reported that the crack growth rate increased with increasing water vapor pressure up to about 0.67 kPa (5 torr) and then became independent of water vapor pressure. They attributed this saturation behavior (above about 0.67 kPa) to

possible capillary condensation of water vapor at the crack tip. The pressure dependence at the lower water vapor pressures is consistent with the fact that the extent of (oxidation) reaction and, hence, the amount of hydrogen production is a function of exposure or pressure. The possibility that capillary condensation might occur at the crack tip raises a question concerning the appropriateness of correlating vapor-solid reaction kinetics with that for crack growth in water vapor at pressures above 0.67 kPa (5 torr) and in (liquid) water. Two observations tend to support the position that such a correlation is indeed appropriate. First, passivation layers of oxide of comparable thickness (equivalent to at most two layers of oxide) were found on the fracture surface following crack growth in water vapor above 0.67 kPa (5 torr) and on a flat steel surface (on which condensation did not take place) following exposure at the same pressure. Second, there is good agreement between the activation energy for the surface reaction with water vapor and that for Stage II crack growth in (liquid) water. These observations suggest that the extent of reaction in water (in the absence of electrochemical influences), as in the case of water vapor, is limited, and that a single reaction mechanism applies to the reaction with water and water vapor.

The reported arrest of crack growth by the presence of oxygen in water vapor [12] appears to be caused by the formation of an oxide layer that inhibits the reaction of water vapor with the steel, which is in agreement with the hypothesis of Hancock and Johnson [12]. The effectiveness of oxygen in stopping crack growth in water vapor results from the fact that the reaction of oxygen with steel (both iron and iron carbide phases) is at least 10^6 times faster than the oxidation reaction in water vapor.

5.0 SUMMARY

Based on the results from coordinated fracture mechanics and surface chemistry studies of the kinetics of crack growth in hydrogen, in water and in water vapor,

and of the kinetics of surface reactions with water vapor on a single material, hydrogen has been identified as the embrittling specie for enhancing subcritical crack growth in these environments for low alloy, carbon martensitic steels. The surface reaction associated with oxidation and the liberation of hydrogen has been unambiguously identified as the rate controlling process for crack growth in water/water vapor. The rate controlling process for crack growth in hydrogen remains to be determined, and could be one of the sequential steps in surface reaction, or hydrogen entry and subsequent transport to the fracture site, or the fracture process itself. The difference in crack growth behavior in water vapor at low and high vapor pressures (below and above about 0.67 kPa) may be related to the effect of pressure on the rate of surface reaction, rather than to a difference in the mechanism of reaction between water vapor and liquid water (resulting from capillary condensation).

The inhibiting effect of oxygen for crack growth in water vapor can be attributed to the formation of an oxide layer by the reaction of oxygen with the surface that precludes the reaction with water vapor to produce hydrogen. The effectiveness of oxygen lies in the fact that its reaction rate with iron (or steel) is at least 10^6 times faster than the oxidation rate for water vapor. This finding is consistent with the earlier hypothesis of Hancock and Johnson [12].

Segregation of alloying or residual impurity elements to the prior austenite grain boundaries does not appear to be essential for a steel to be susceptible to environment assisted subcritical crack growth. The role of such segregation in further enhancing the susceptibility still needs to be identified and understood.

Acknowledgement

The authors wish to express their appreciation to the United States Steel Corporation for providing the steel and iron carbide used in this investigation, and to Dr. Thomas G. Nilan for his assistance in obtaining the iron carbide specimen. Support of this research by the Office of Naval Research, under Contract N00014-75-C-0543, NR 036-097, and by the National Science Foundation, under Grants DMR74-10489 and DMR76-21624, is gratefully acknowledged. Assistance with the fracture mechanics experiments by Messrs. Yukata Mizuta, Jean-Pierre Hutin and C. D. Miller is also acknowledged.

References

1. H. H. Johnson and A. M. Willner: Appl. Mater. Res., 1965, Vol. 4, P. 34.
2. H. H. Johnson and P. C. Paris: J. Eng. Frac. Mech., 1968, Vol. 1, P. 3.
3. R. P. Wei: Proceedings of Conference-Fundamental Aspects of Stress Corrosion Cracking, P. 104, NACE, 1969.
4. R. P. Wei, S. R. Novak, and D. P. Williams: Mater. Res. Stand., 1972, Vol. 12, P. 25.
5. H. G. Nelson and D. P. Williams: Met. Trans., 1970, Vol. 1, P. 63.
6. H. G. Nelson, D. P. Williams, and A. S. Tetelman: Met. Trans., 1971, Vol. 2, P. 953.
7. J. D. Landes and R. P. Wei: Int. J. Frac., 1973, Vol. 9, P. 277.
8. S. J. Hudak and R. P. Wei: Met. Trans. A, 1976, Vol. 7A, P. 235.
9. R. P. Gangloff and R. P. Wei: Met. Trans. A, 1977, Vol. 8A, P. 1043.
10. W. A. Van der Sluys: J. Eng. Fract. Mech., 1969, Vol. 1, P. 447.
11. H. H. Johnson: Stress Corrosion Cracking and Hydrogen Embrittlement in Iron Based Alloys, J. Hochmann, J. Slater, and R. W. Staehle, eds., in press, NACE, Houston, Texas.
12. G. G. Hancock and H. H. Johnson: Trans. AIME, 1966, Vol. 236, P. 513.
13. W. K. Wilson: Westinghouse Research Laboratories, Report No. 67-707-BTLPV-R1, 1967.
14. J. P. Hutin and Y. Mizuta: Lehigh University, Bethlehem, Pennsylvania, unpublished research, 1975.
15. R. P. Wei and G. W. Simmons: Scr. Met., 1976, Vol. 10, P. 153.
16. P. C. Paris and G. C. Sih: in Fracture Toughness Testing and Its Applications, ASTM STP 381, P. 30, ASTM, Philadelphia, PA., 1965.
17. G. W. Simmons and D. J. Dwyer: Surface Sci., 1975, Vol. 48, P. 373.
18. D. J. Dwyer, G. W. Simmons, and R. P. Wei: Surface Sci., 1977, Vol. 64, P. 617.
19. H. G. Nelson and D. P. Williams: Stress Corrosion Cracking and Hydrogen Embrittlement of Iron Based Alloys, J. Hochmann, J. Slater, and R. W. Staehle, eds., in press, NACE, Houston, Texas.
20. J. D. Landes and R. P. Wei: J. Eng. Matls. Tech., 1973, Vol. 95, ser. H., P. 2.
21. I. M. Bernstein: Met. Trans., 1970, Vol. 1, P. 3143.
22. M. L. Wayman and G. C. Smith: Met. Trans., 1970, Vol. 1, P. 1189.

23. B. B. Rath and I. M. Bernstein: Met. Trans., 1972, Vol. 2, P. 2845.

24. I. M. Bernstein: Mater. Sci. Eng., 1970, Vol. 6, P. 1.

25. A. Joshi and D. F. Stein: in Temper Embrittlement of Low Alloy Steels, ASTM, STP 499, 1972, P. 59.

26. A. Joshi, L. E. Davis and P. W. Palmberg: in Methods of Surface Analysis, ed., A. W. Czanderna, Elsevier Publishing Co., N.Y., 1975.

27. Melvin Avrami: J. Chem. Phys., 1939, Vol. 7, P. 1103.

28. Melvin Avrami: J. Chem. Phys., 1940, Vol. 8, P. 212

29. Melvin Avrami: J. Chem. Phys., 1941, Vol. 9, P. 117.

30. William A. Johnson and Robert F. Mehl: Trans. AIME, 1939, Vol. 135, P. 416.

31. R. Suhrmann, J. M. Heras, L. Viscido De Heras and G. Wedler: Ber. Bunsenges. Physil. Chem., 1969, Vol. 72, P. 855.

32. D. Lazarov and G. Bliznakov: Z. Physik. Chem., 1966, Vol. 233, P. 255.

33. G. M. Kornacheva, R. Kh. Burshtein and N. A. Shurmovskaya: Electrochimiya, 1973, Vol. 9, P. 81.

34. S. Chang and W. H. Wade: J. Colloid Interface Sci., 1970, Vol. 34, P. 413.

35. K. Kishi and S. Ikeda: Bull. Chem. Soc. Japan, 1973, Vol. 46, P. 341.

FIGURE CAPTIONS

Figure 1: The kinetics of sustained-load crack growth in AISI 4340 steel (tempered at 205°C) in dehumidified hydrogen at 133 kPa.

Figure 2: Effect of temperature on the rate of Stage II (rate limited) crack growth in AISI 4340 steel (tempered at 205°C) in dehumidified hydrogen at 133 kPa.

Figure 3: The kinetics of sustained-load crack growth in AISI 4340 steel (tempered at 205°C) in distilled water [7,14].

Figure 4: Effect of temperature on the rate of Stage II (rate limited) crack growth in AISI 4340 steel (tempered at 205°C) in distilled water.

Figure 5: Tracing of load-time record to indicate crack growth response as a function of water vapor pressure.

Figure 6: Representative SEM fractographs of AISI 4340 steel fracture by crack growth at $K = 33$ MPa-$m^{1/2}$: (a) in hydrogen at 133 kPa and 22.2°C, and (b) in distilled water at 0°C.

Figure 7: Representative SEM fractographs of AISI 4340 steel specimens: (a) fractured by crack growth in water vapor below 0.67 kPa at room temperature, and (b) fractured by overload at room temperature.

Figure 8: Auger electron spectra obtained from fracture surfaces of AISI 4340 steel specimens fractured by <u>in situ</u> crack growth: (a) in hydrogen at 53.2 kPa and - 30°C, (b) in water vapor at 0.67 kPa, and (c) in water vapor at less than 0.67 kPa.

Figure 9: Oxygen Auger electron signal from AISI 4340 steel surface as a function of exposure to water vapor at three temperatures. (The steel surface was ion etched prior to each exposure to water vapor.)

Figure 10: Fraction of surface converted to oxide as a function of exposure.

Figure 11: Effect of temperature on the rate of reaction of water vapor with AISI 4340 steel surface.

Figure 12: Oxygen Auger electron signal from AISI 4340 steel surface as a function of exposure to oxygen at room temperature.

Figure 13: SEM micrographs of ion-etched surface of an iron carbide/iron specimen.

Figure 14: Auger electron spectra obtained from (a) iron carbide/iron specimen during ion etching, (b) iron carbide/iron specimen following exposure to water vapor at 0.67 kPa and room temperature, and (c) polycrystalline pure iron specimen exposed to water vapor at the same time.

Figure 15: Carbon Auger electron peak before (a) and after (b) exposure to water vapor.

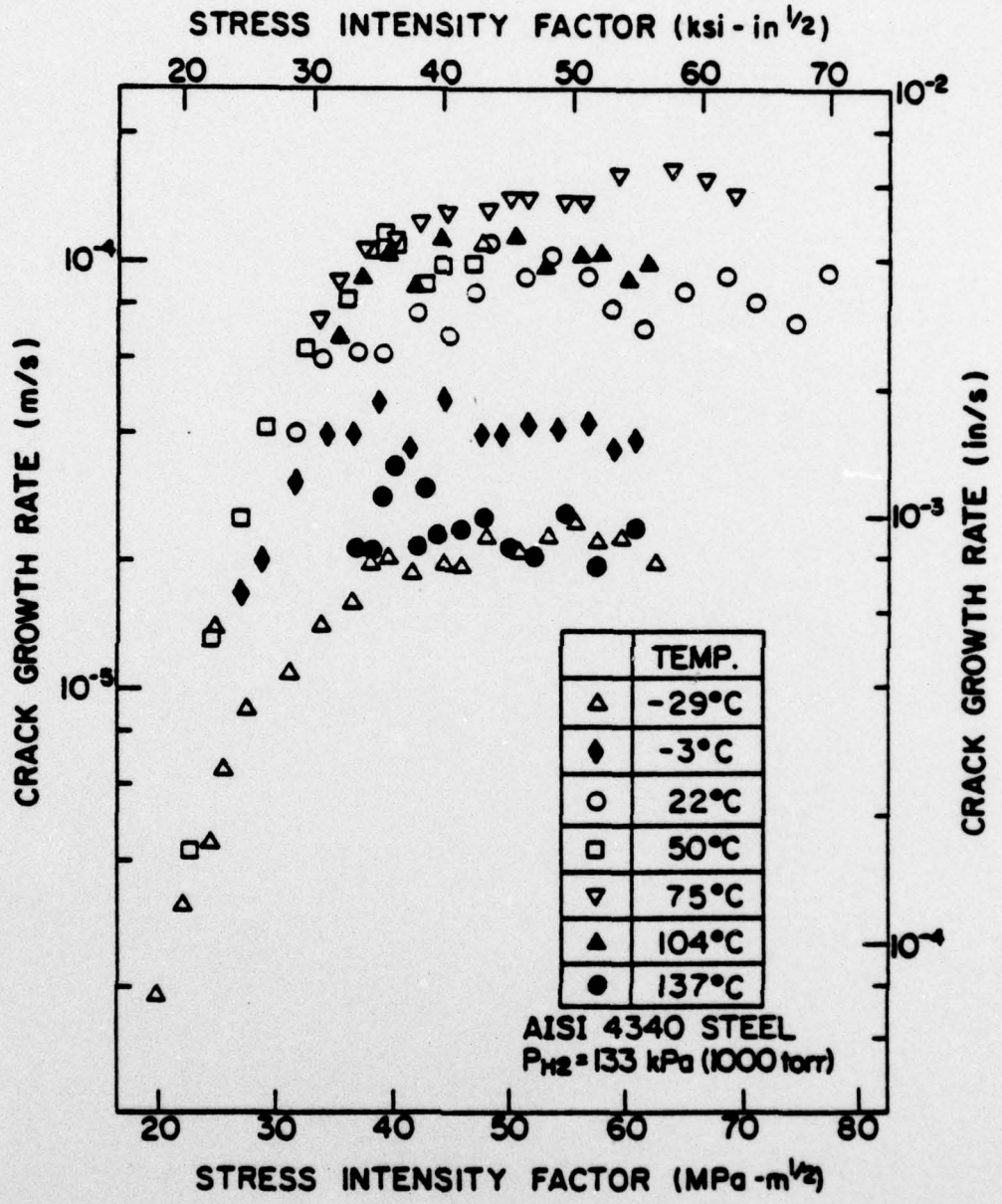

Figure 1: The kinetics of sustained-load crack growth in AISI 4340 steel (tempered at 205°C) in dehumidified hydrogen at 133 kPa.

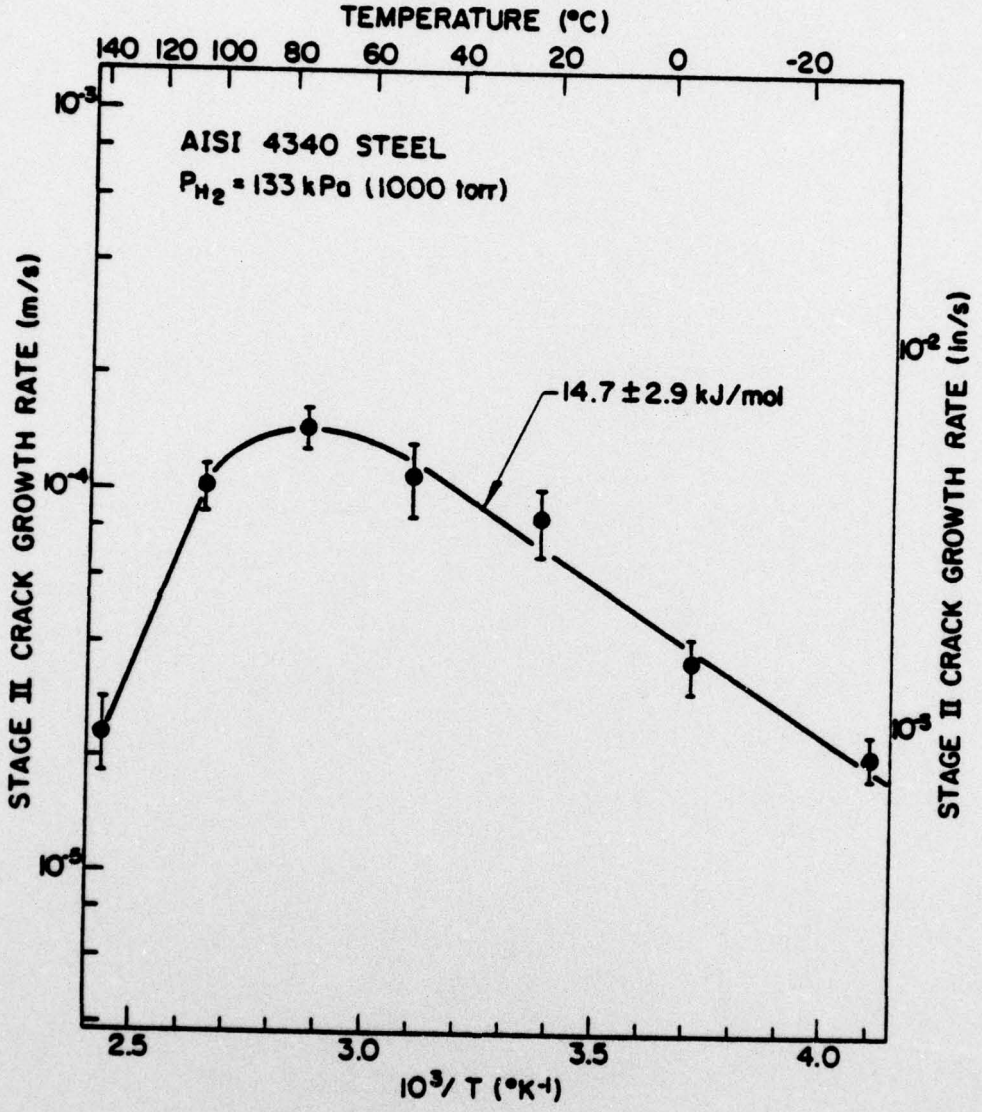

Figure 2: Effect of temperature on the rate of Stage II (rate limited) crack growth in AISI 4340 steel (tempered at 205°C) in dehumidified hydrogen at 133 kPa.

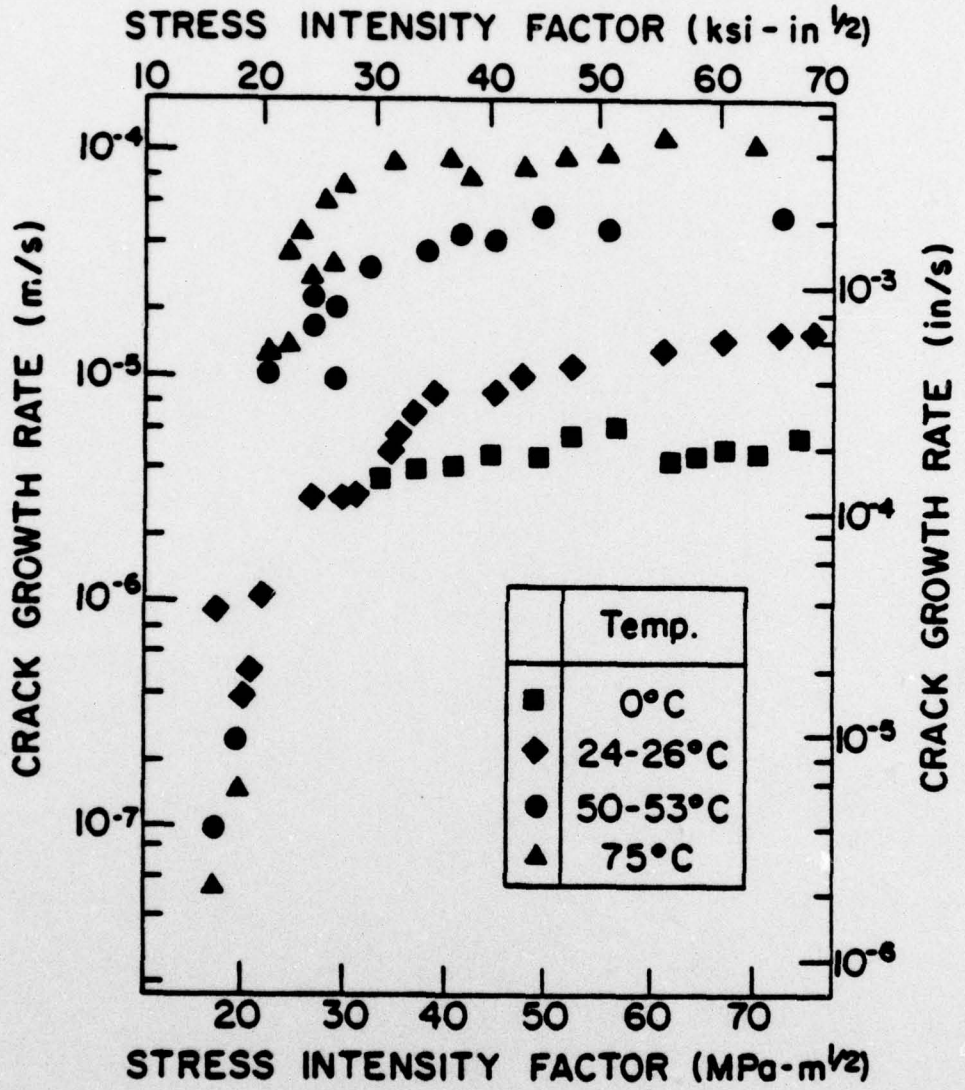

Figure 3: The kinetics of sustained-load crack growth in AISI 4340 steel (tempered at 205°C) in distilled water [7,14].

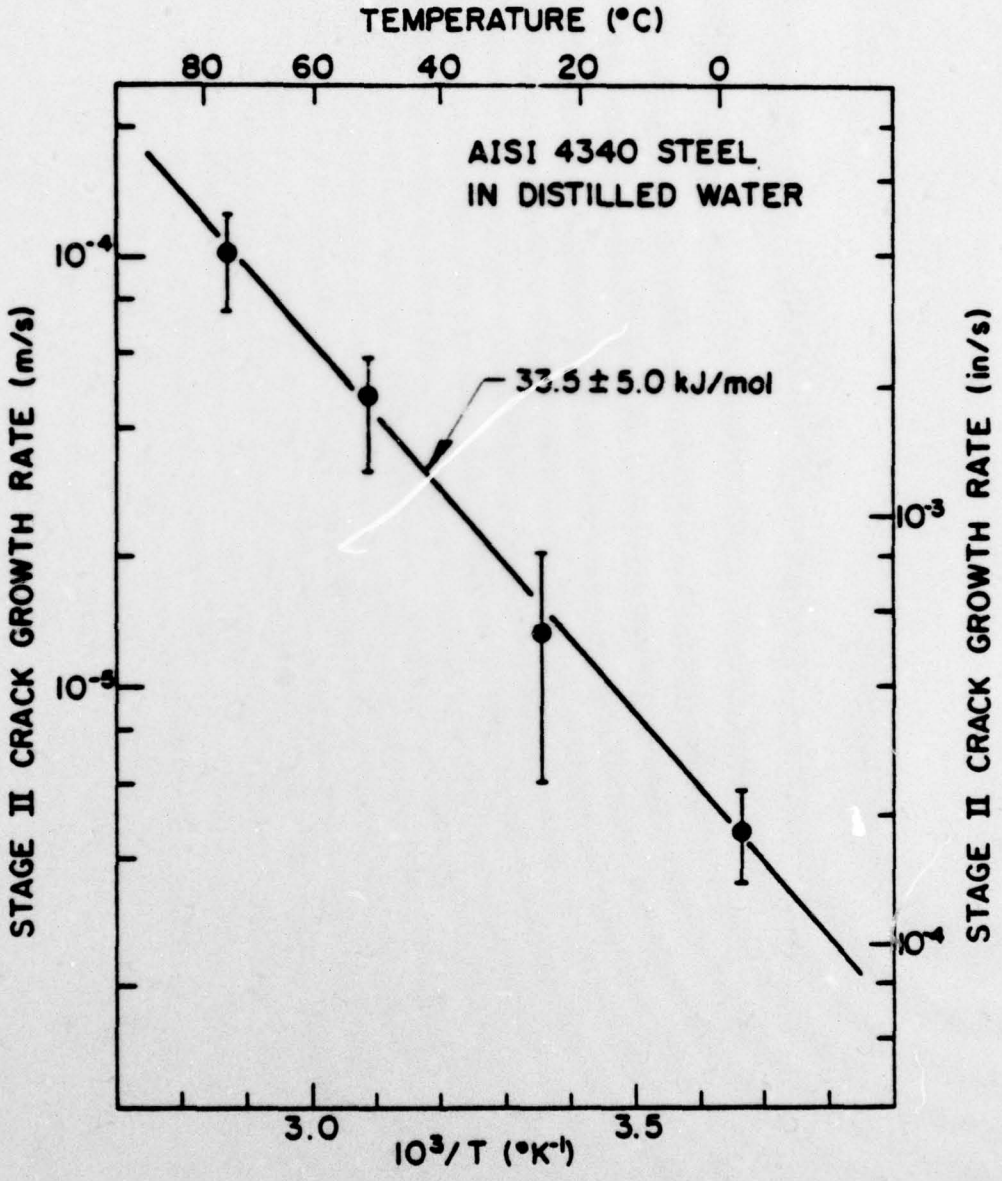

Figure 4: Effect of temperature on the rate of Stage II (rate limited) crack growth in AISI 4340 steel (tempered at 205°C) in distilled water.

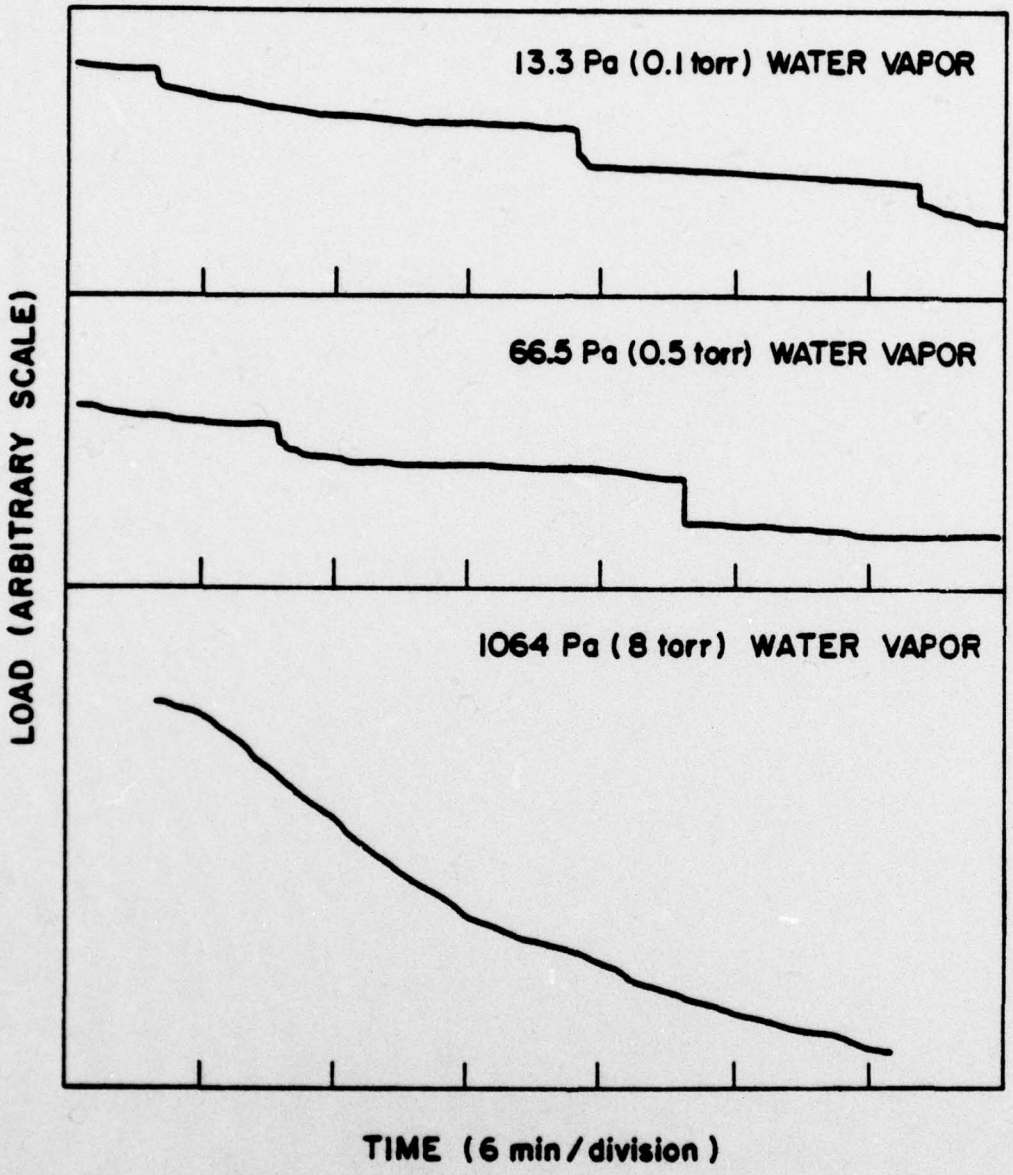

Figure 5: Tracing of load-time record to indicate crack growth response as a function of water vapor pressure.

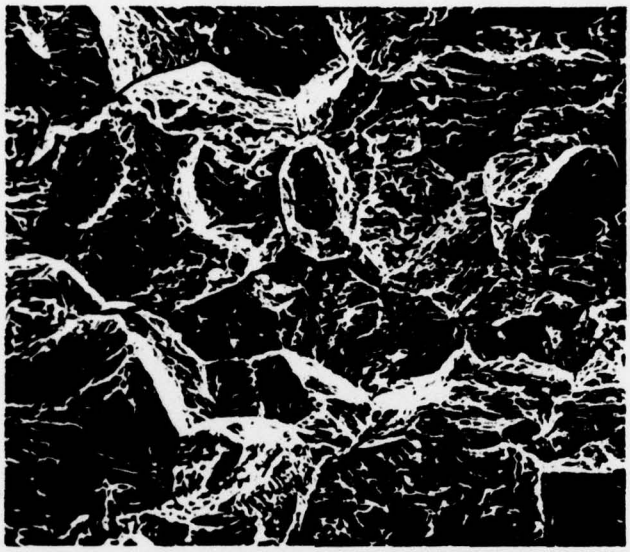

(a) 800X

(b) 800X

Figure 6: Representative SEM fractographs of AISI 4340 steel fractured by crack growth at $K \approx 33$ MPa-$m^{1/2}$: (a) in hydrogen at 133 kPa and 22.2°C, and (b) in distilled water at 0°C.

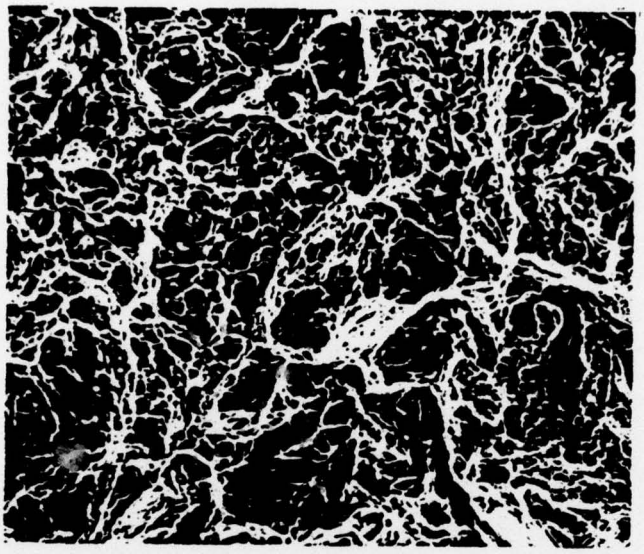

(a) 800X

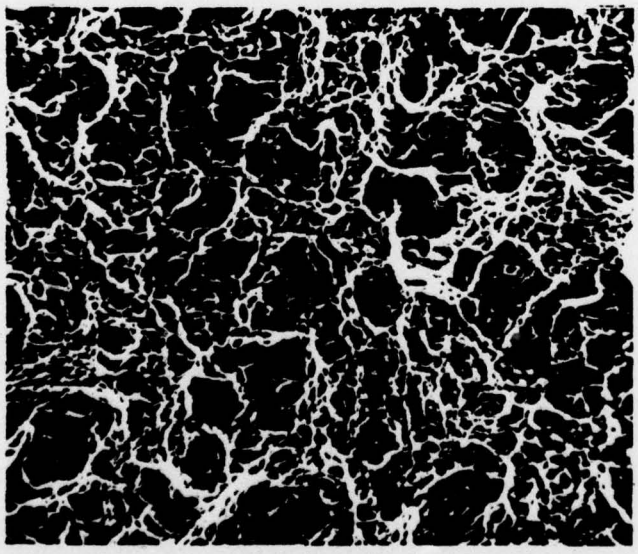

(b) 800X

Figure 7: Representative SEM fractographs of AISI 4340 steel specimens: (a) fractured by crack growth in water vapor below 0.67 kPa at room temperature, and (b) fractured by overload at room temperature.

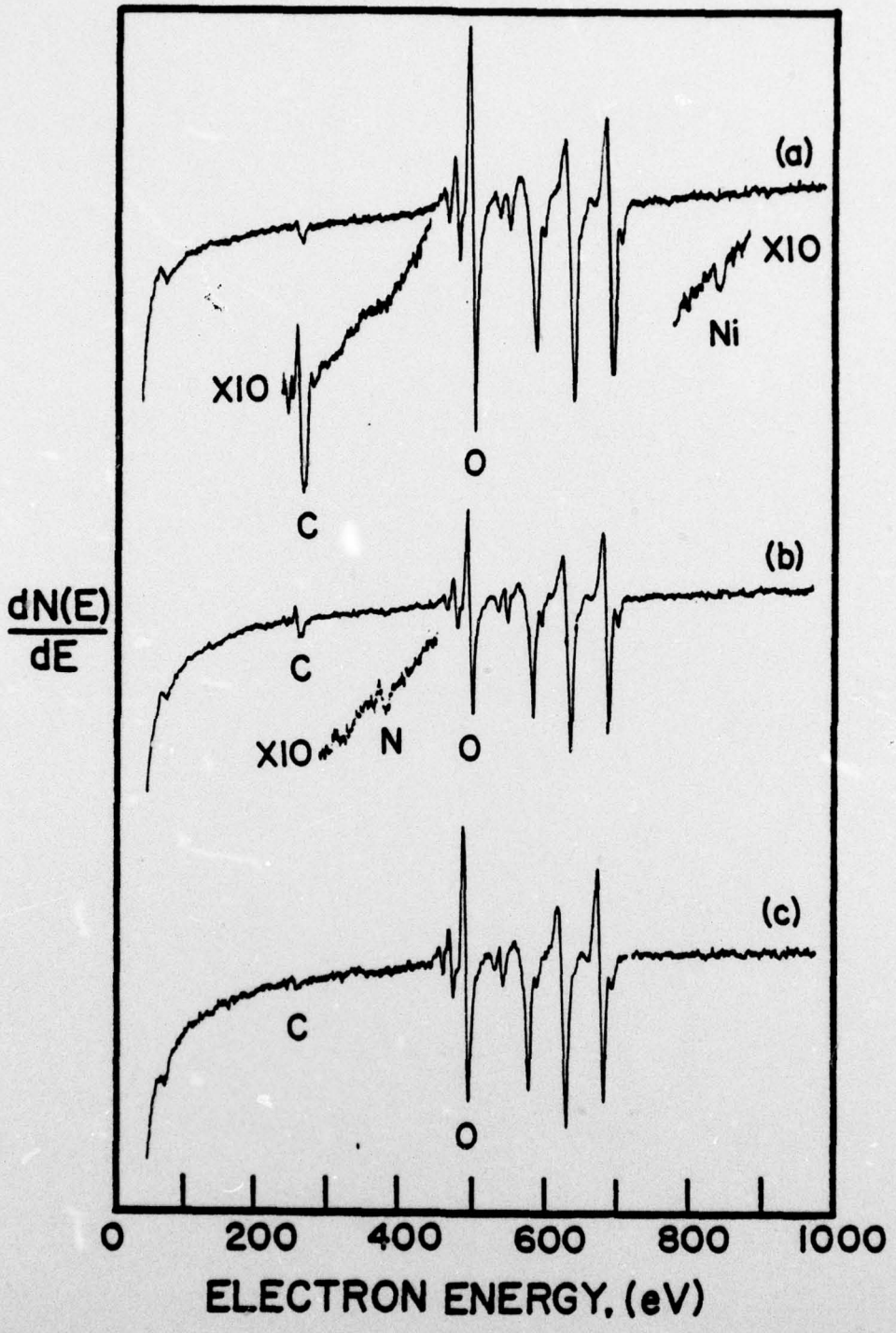

Figure 8: Auger electron spectra obtained from fracture surfaces of AISI 4340 steel specimens fractured by in situ crack growth: (a) in hydrogen at 53.2 kPa and - 30°C, (b) in water vapor at 0.67 kPa, and (c) in water vapor at less than 0.67 kPa.

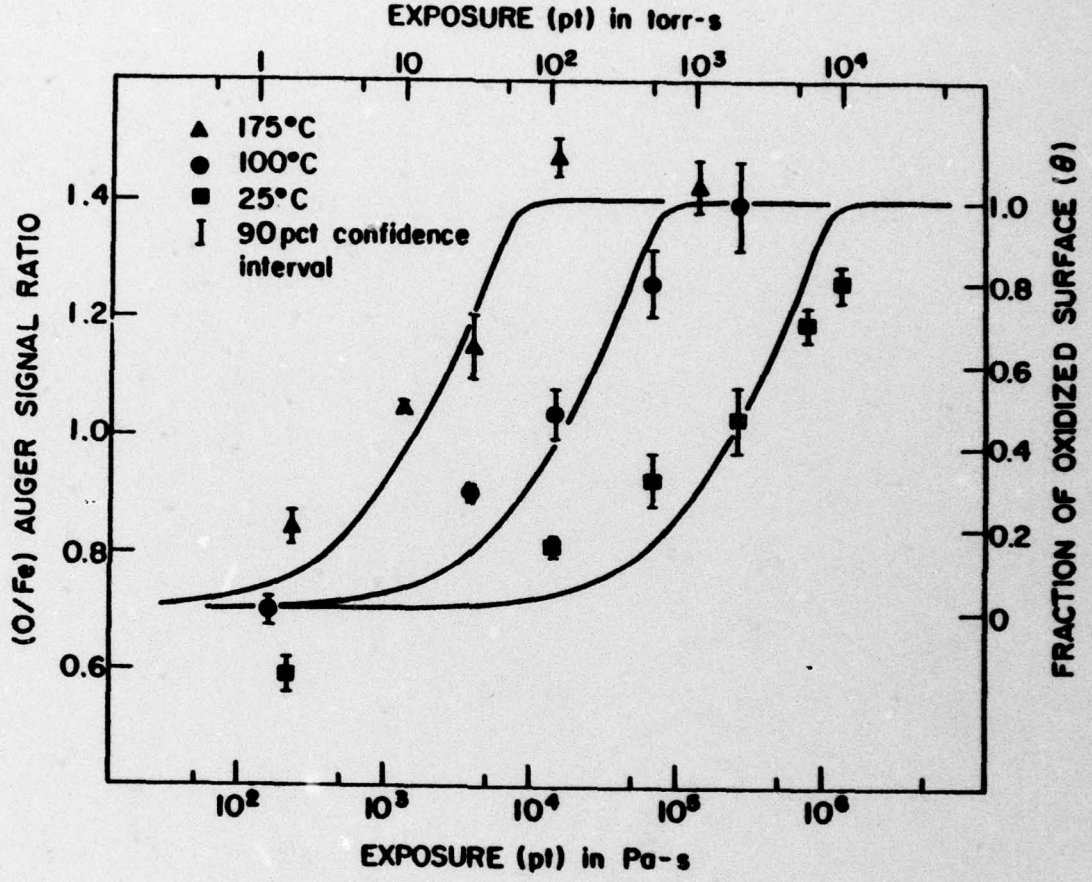

Figure 9: Oxygen Auger electron signal from AISI 4340 steel surface as a function of exposure to water vapor at three temperatures. (The steel surface was ion etched prior to each exposure to water vapor.)

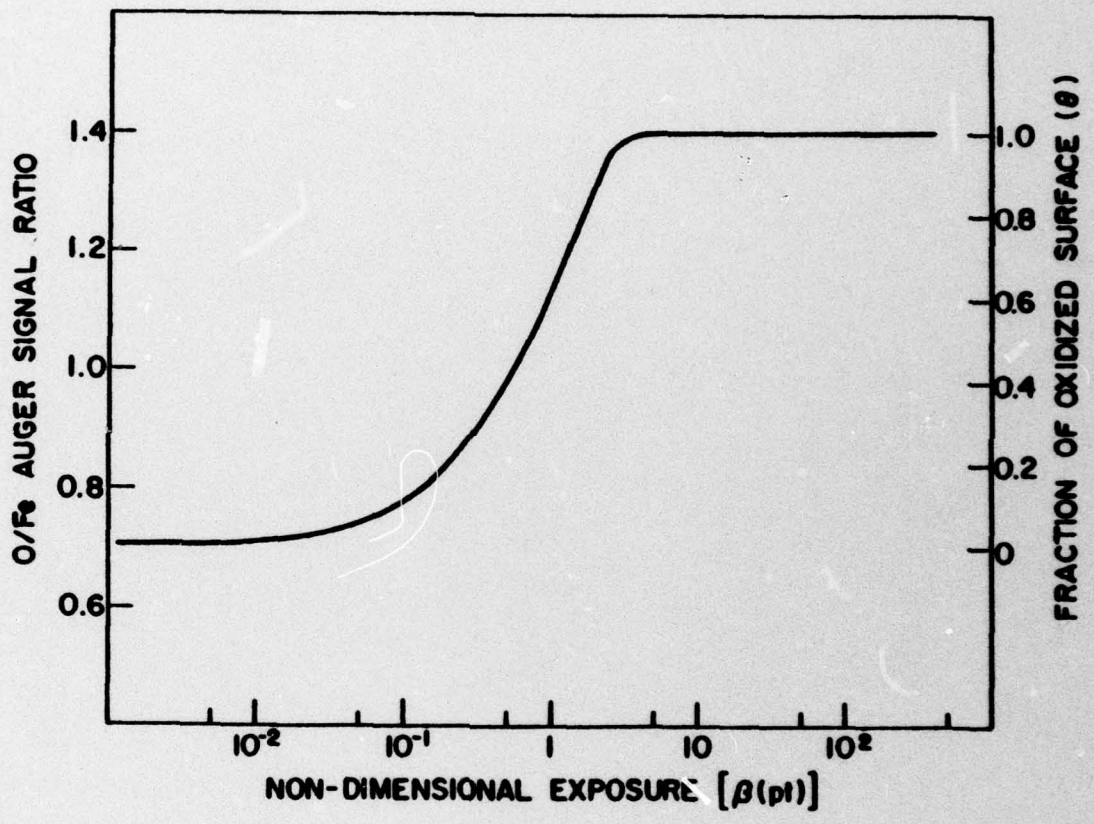

Figure 10: Fraction of surface converted to oxide as a function of exposure.

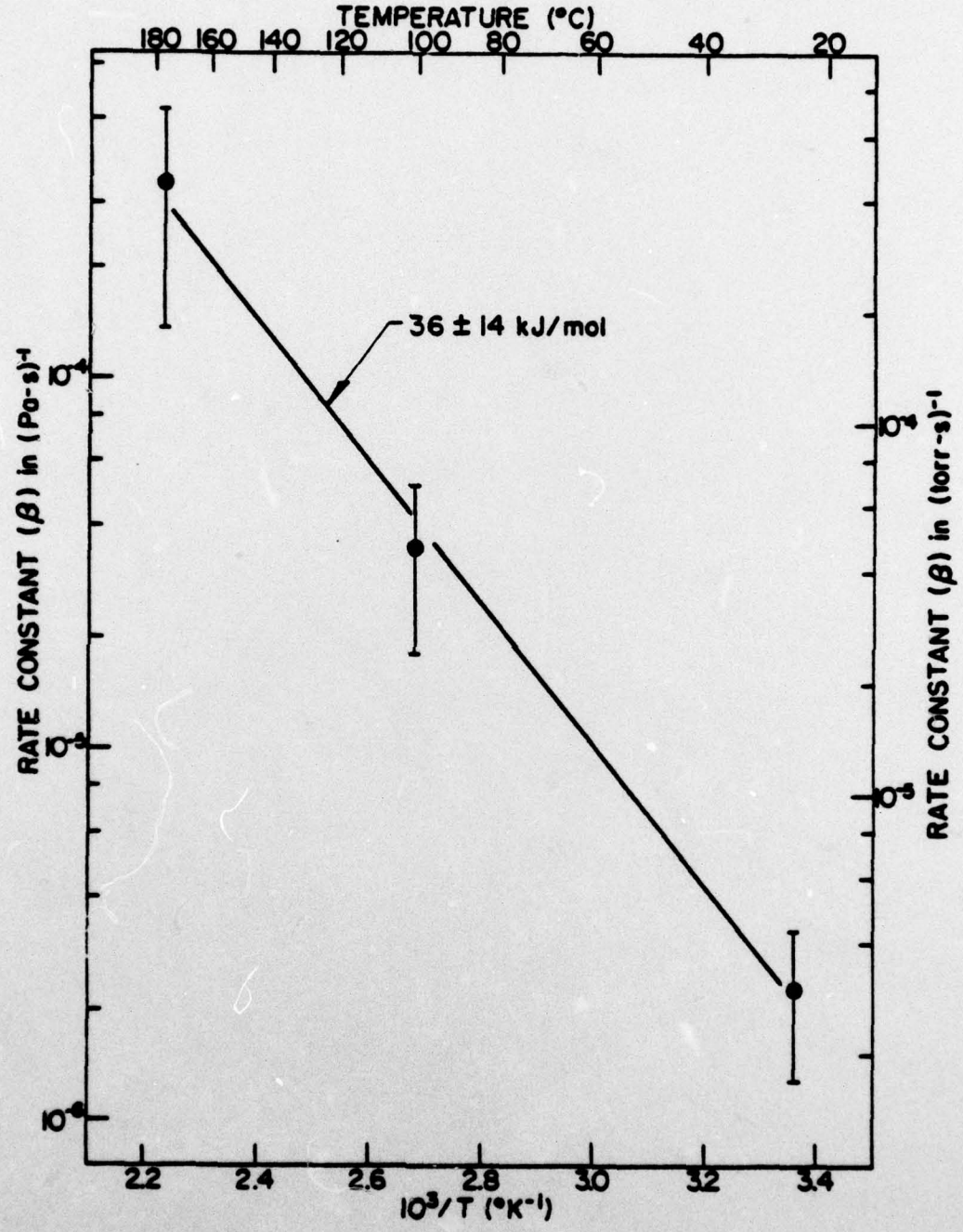

Figure 11: Effect of temperature on the rate of reaction of water vapor with AISI 4340 steel surface.

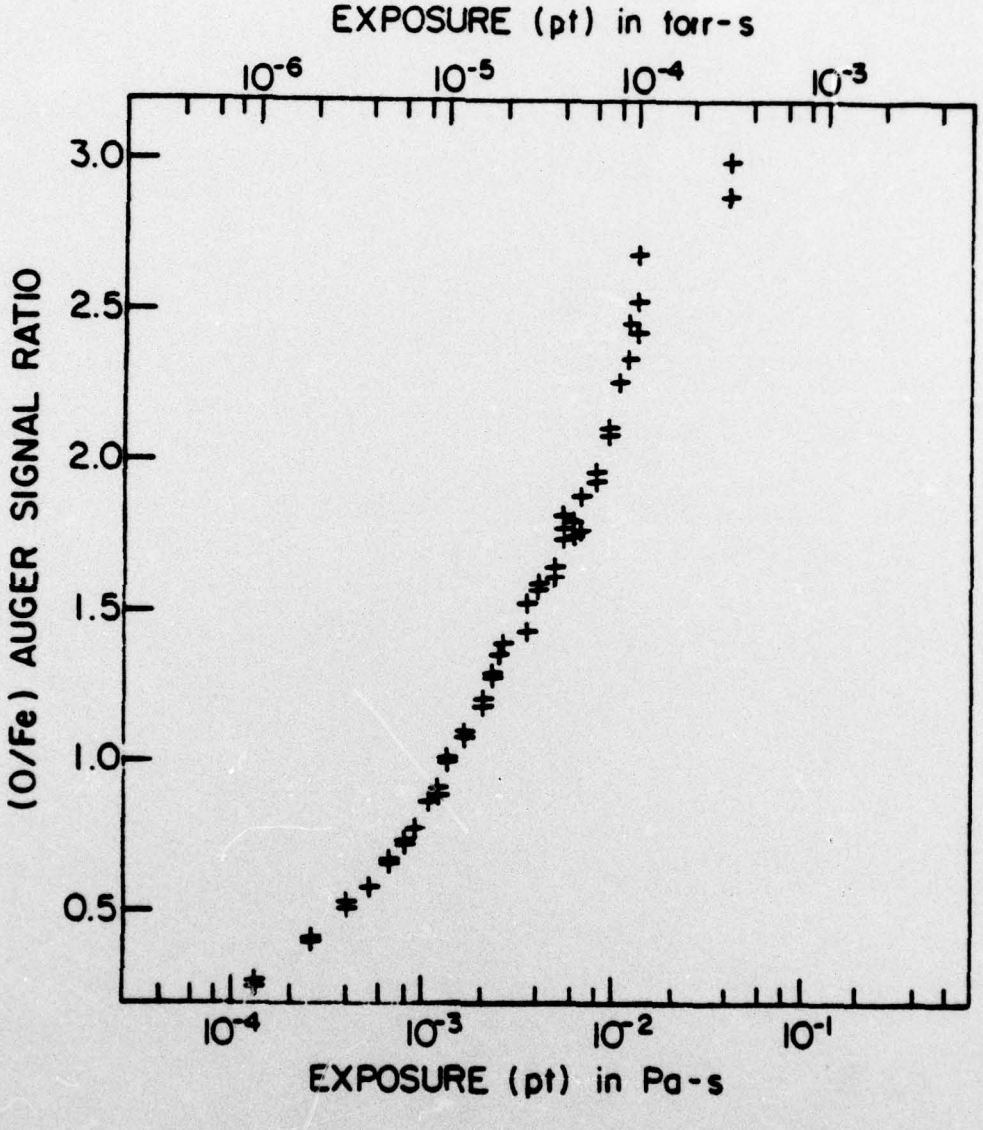

Figure 12: Oxygen Auger electron signal from AISI 4340 steel surface as a function of exposure to oxygen at room temperature.

(a) 150X

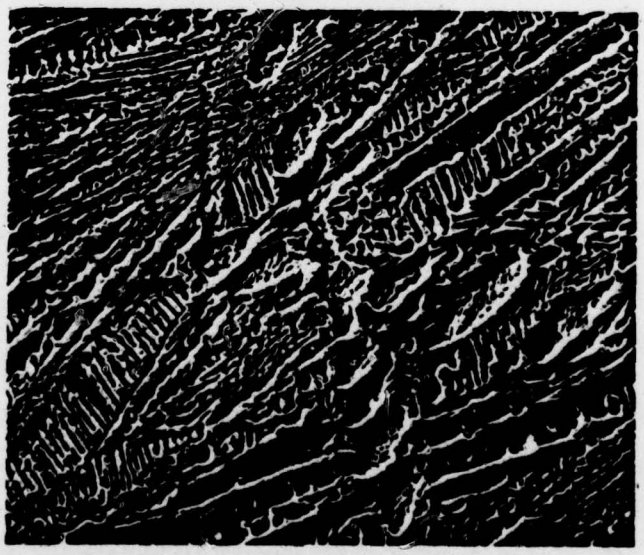

(b) 600X

Figure 13: SEM micrographs of ion-etched surface of an iron carbide/iron specimen.

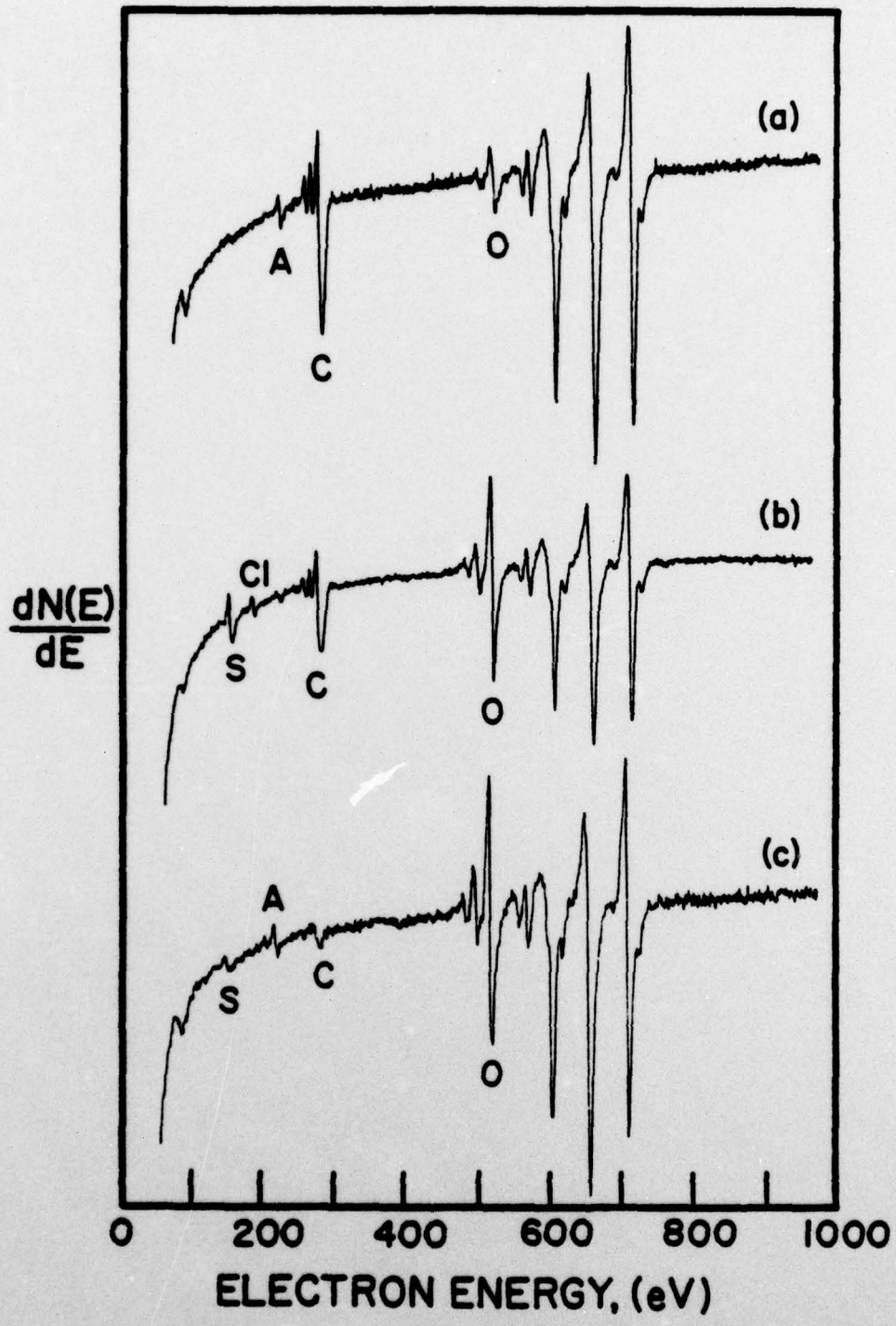

Figure 14: Auger electron spectra obtained from (a) iron carbide/iron specimen during ion etching, (b) iron carbide/iron specimen following exposure to water vapor at 0.67 kPa and room temperature, and (c) polycrystalline pure iron specimen exposed to water vapor at the same time.

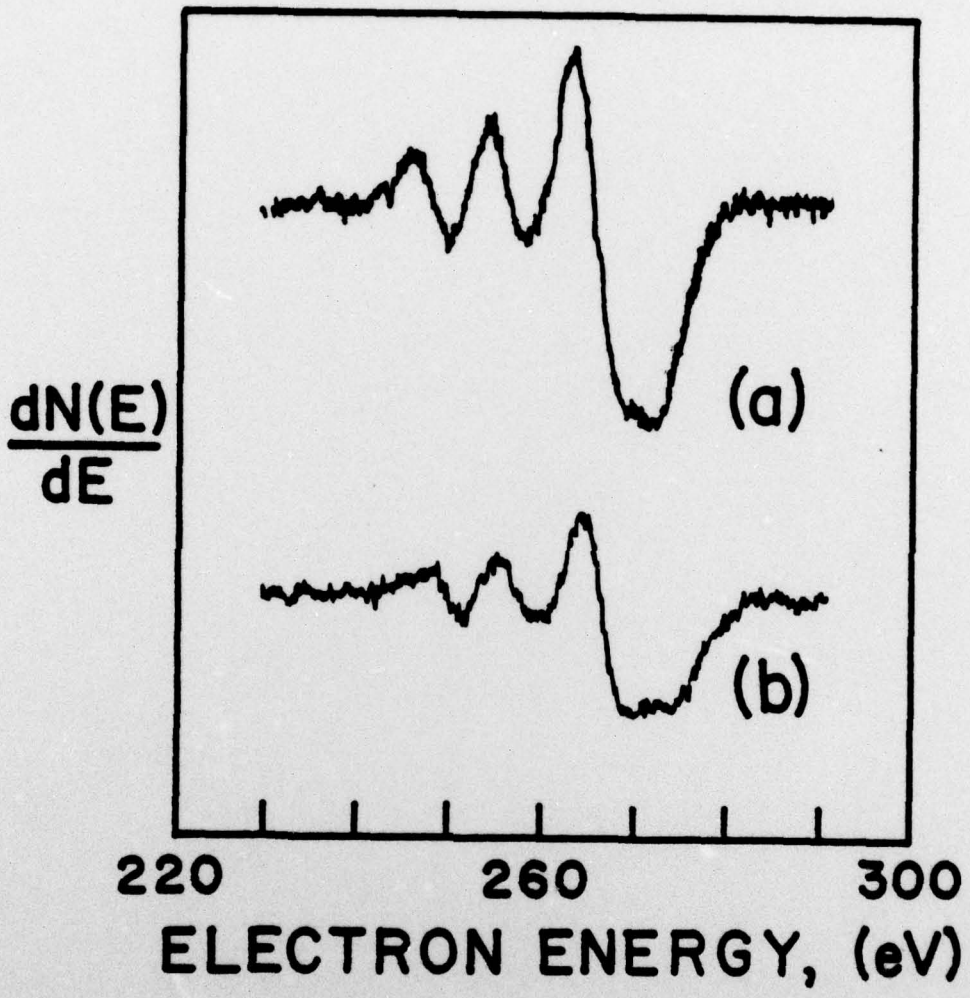

Figure 15: Carbon Auger electron peak before (a) and after (b) exposure to water vapor.

BASIC DISTRIBUTION LIST

October 1976

Technical and Summary Reports

Organization	No. of Copies
Defense Documentation Center Cameron Station Alexandria, Virginia 22314	(12)
Office of Naval Research Department of the Navy	
Attn: Code 471	(1)
Code 102	(1)
Code 470	(1)
Commanding Officer Office of Naval Research Branch Office 495 Summer Street Boston, Massachusetts 02210	(1)
Commanding Officer Office of Naval Research Branch Office 536 South Clark Street Chicago, Illinois 60605	(1)
Office of Naval Research San Francisco Area Office 760 Market Street, Room 447 San Francisco, California 94102 Attn: Dr. P. A. Miller	(1)
Naval Research Laboratory Washington, D.C. 20390	
Attn: Code 6000	(1)
Code 6100	(1)
Code 6300	(1)
Code 6400	(1)
Code 2627	(1)
Naval Air Development Center Code 302 Warminster, Pennsylvania 18974 Attn: Mr. F. S. Williams	(1)
Naval Air Propulsion Test Center Trenton, New Jersey 08628 Attn: Library	(1)
Naval Construction Batallion Civil Engineering Laboratory Port Hueneme, California 93043 Attn: Materials Division	(1)
Naval Electronics Laboratory Center San Diego, California 92152 Attn: Electron Materials Sciences Division	(1)
Naval Missile Center Materials Consultant Code 3312-1 Point Mugu, California 93041	(1)
Commanding Officer Naval Surface Weapons Center White Oak Laboratory Silver Spring, Maryland 20910 Attn: Library	(1)
David W. Taylor Naval Ship R&D Center Materials Department Annapolis, Maryland 21402	(1)
Naval Undersea Center San Diego, California 92132 Attn: Library	(1)
Naval Underwater System Center Newport, Rhode Island 02840 Attn: Library	(1)
Naval Weapons Center China Lake, California 93555 Attn: Library	(1)
Naval Postgraduate School Monterey, California 93940 Attn: Mechanical Engineering Dept.	(1)
Naval Air Systems Command Washington, D.C. 20360	
Attn: Code 52031	(1)
Code 52032	(1)
Code 320	(1)

Organization	No. of Copies
Naval Sea System Command Washington, D.C. 20362 Attn: Code 035	(1)
Naval Facilities Engineering Command Alexandria, Virginia 22331 Attn: Code 03	(1)
Scientific Advisor Commandant of the Marine Corps Washington, D.C. 20380 Attn: Code AX	(1)
Naval Ship Engineering Center Department of the Navy CTR BG #2 3700 East-West Highway Prince Georges Plaza Hyattsville, Maryland 20782 Attn: Engineering Materials and Services Office, Code 6101	(1)
Army Research Office Box CM, Duke Station Durham, North Carolina 27706 Attn: Metallurgy & Ceramics Div.	(1)
Army Materials and Mechanics Research Center Watertown, Massachusetts 02172 Attn: Res. Programs Office (AMXMR-P)	(1)
Air Force Office of Scientific Research Bldg. 410 Bolling Air Force Base Washington, D.C. 20332 Attn: Chemical Science Directorate Electronics and Solid State Sciences Directorate	(1) (1)
Air Force Materials Lab (LA) Wright-Patterson AFB Dayton, Ohio 45433	(1)
NASA Headquarters Washington, D.C. 20546 Attn: Code RRM	(1)
NASA Lewis Research Center 21000 Brookpark Road Cleveland, Ohio 44135 Attn: Library	(1)
National Bureau of Standards Washington, D.C. 20234 Attn: Metallurgy Division Inorganic Materials Division	(1) (1)
Defense Metals and Ceramics Information Center Battelle Memorial Institute 505 King Avenue Columbus, Ohio 43201	(1)
Director Ordnance Research Laboratory P.O. Box 30 State College, Pennsylvania 16801	(1)
Director Applied Physics Laboratory University of Washington 1013 Northeast Fortieth Street Seattle, Washington 98105	(1)
Metals and Ceramics Division Oak Ridge National Laboratory P.O. Box X Oak Ridge, Tennessee 37380	(1)
Los Alamos Scientific Laboratory P.O. Box 1663 Los Alamos, New Mexico 87544 Attn: Report Librarian	(1)
Argonne National Laboratory Metallurgy Division P.O. Box 229 Lemont, Illinois 60439	(1

Organization	No. of Copies	Organization	No. of Copies
Brookhaven National Laboratory Technical Information Division Upton, Long Island New York 11973 Attn: Research Library	(1)		
Library Building 50 Room 134 Lawrence Radiation Laboratory Berkeley, California	(1)		

C
July 1977

SUPPLEMENTARY DISTRIBUTION LIST

Technical and Summary Reports

Dr. T. R. Beck
Electrochemical Technology Corporation
10035 31st Avenue, NE
Seattle, WA 98125

Professor I. M. Bernstein
Carnegie-Mellon University
Schenley Park
Pittsburgh, PA 15213

Professor H. K. Birnbaum
University of Illinois
Department of Metallurgy
Urbana, IL 61801

Dr. Otto Buck
Rockwell International
1049 Camino Dos Rios
P.O. Box 1085
Thousand Oaks, CA 91360

Dr. David L. Davidson
Southwest Research Institute
8500 Culebra Road
P.O. Drawer 28510
San Antonio, TX 78284

Dr. D. J. Duquette
Department of Metallurgical Engineering
Rensselaer Polytechnic Institute
Troy, NY 12181

Professor R. T. Foley
The American University
Department of Chemistry
Washington, DC 20016

Mr. G. A. Gehring
Ocean City Research Corporation
Tennessee Avenue & Beach Thorofare
Ocean City, NJ 08226

Dr. J. A. S. Green
Martin Marietta Corporation
1450 South Rolling Road
Baltimore, MD 21227

Professor R. H. Heidersbach
University of Rhode Island
Department of Ocean Engineering
Kingston, RI 02881

Professor H. Herman
State University of New York
Material Sciences Division
Stony Brook, NY 11794

Professor J. P. Hirth
Ohio State University
Metallurgical Engineering
Columbus, OH 43210

Dr. D. W. Hoeppner
University of Missouri
College of Engineering
Columbia, MO 65201

Dr. E. W. Johnson
Westinghouse Electric Corporation
Research and Development Center
1310 Beulah Road
Pittsburgh, PA 15235

Dr. F. Mansfeld
Rockwell International Science Center
1049 Camino Dos Rios
P.O. Box 1085
Thousand Oaks, CA 91360

Professor A. E. Miller
University of Notre Dame
College of Engineering
Notre Dame, IN 46556

Dr. Jeff Perkins
Naval Postgraduate School
Monterey, CA 93940

Professor H. W. Pickering
Pennsylvania State University
Department of Material Sciences
University Park, PA 16802

C
July 1977

SUPPLEMENTARY DISTRIBUTION LIST
(Continued)

Dr. William R. Prindle
National Academy of Sciences
National Research Council
2101 Constitution Avenue
Washington, DC 20418

Professor R. W. Staehle
Ohio State University
Department of Metallurgical Engineering
Columbus, OH 43210

Dr. Barry C. Syrett
Stanford Research Institute
333 Ravenswood Avenue
Menlo Park, CA 94025

Dr. R. P. Wei
Lehigh University
Institute for Fracture and
Solid Mechanics
Bethlehem, PA 18015

Professor H. G. F. Wilsdorf
University of Virginia
Department of Materials Science
Charlottesville, VA 22903

AD-A045 532 LEHIGH UNIV BETHLEHEM PA INST OF FRACTURE AND SOLID --ETC F/G 11/6
FRACTURE MECHANICS AND SURFACE CHEMISTRY STUDIES OF SUBCRITICAL--ETC(U)
SEP 77 G W SIMMONS, P S PAO, R P WEI N00014-75-C-0543

UNCLASSIFIED IFSM-77-83 NL

2 OF 2
AD
A045532

END
DATE FILMED
1-78
DDC

SUPPLEMENTARY

INFORMATION

AD- A045532

LEHIGH UNIVERSITY

Bethlehem, Pennsylvania 18015

Department of
Mechanical Engineering & Mechanics
Building No. 19

November 16, 1977

Dr. P. A. Clarkin Code 471
Metallurgy Program
Office of Naval Research
Department of the Navy
Arlington, VA.

Re: Met. Trans. A
77-348-E

Dear Phil:

We have discovered an unfortunate error on pages 16 and 19 of the referenced paper. The escape depth for oxygen Auger electrons was given incorrectly as 70 nm instead of 0.7 nm. Would you please make the corrections in your copy of the report? By a copy of this letter, the errata sheet is being sent to individuals and organizations on the Distribution List.

Best regards.

Sincerely yours,

Bob

R. P. Wei

RPW:ss

ERRATA SHEET

Report Number: IFSM-77-83

"Fracture Mechanics and Surface Chemistry Studies of Subcritical Crack Growth in AISI 4340 Steel" by G. W. Simmons, P. S. Pao and R. P. Wei, Lehigh University, Bethlehem, PA.

Contract N00014-75-C-0543, NR 036-097

Date: September, 1977

Page 16	(last line on page)	Change from 70 nm TO 0.7 nm
Page 19	(line #13)	Change from (∿70 nm) TO (∿0.7 nm)